RESEARCH ARTICLE

WILEY

On the process of fine sediment infiltration into static gravel bed: A CFD–DEM modelling perspective

Atul Jaiswal [ORCID] | Minh Duc Bui | Peter Rutschmann

Department of Hydraulic and Water Resources Engineering, Technical University of Munich (TUM), Munich, Germany

Correspondence
Atul Jaiswal, Department of Hydraulic and Water Resources Engineering, Technical University of Munich (TUM), Arcisstr. 21, 80333, Munich, Germany.
Email: atul.jaiswal@tum.de

Abstract

The gravel bed clogging, caused by infiltration and accumulation of fine sediment, degrades the river ecology. A proper understanding of the infiltration process, and underlying mechanism and causes, are necessary to take preventive measures. The process of fine sediment infiltration into static gravel bed is studied by distinguishing between bridging and percolation behaviours, as they affect the river ecology and physical processes occurring in the river system differently. However, several contradicting observations, concerning their occurrences, are reported. We employed the unresolved CFD–DEM method to simulate and investigate the infiltration process. The theoretical size ratios, corresponding to different geometrical configurations for a binary mixture of mono-disperse spherical particles, representing bridging and percolation processes, are considered and simulated with and without flowing water effects. The effects of several turbulence models on the infiltration process are also studied. We found that fine sediment infiltration in fluvial deposits is mainly gravity-dominated, supporting Cui's hypothesis that fine sediment infiltration through intra-gravel flow is similar to fine sediment infiltration driven by gravity. In contrast to consensus in the field, our results demonstrate that the occurrences of different infiltration processes (bridging and percolation) seem to be independent of gravel bed thickness, rather depend only on the relative grain size distribution of fine sediment and gravel. However, a precise definition of a 'thick enough' gravel bed is necessary to distinguish between bridging and percolation behaviours. Here, we hypothesize a suitable gravel bed thickness, which might be regarded as a 'thick enough' gravel bed.

KEYWORDS
bridging, fine sediment infiltration, static gravel bed, unimpeded static percolation, unresolved CFD–DEM

1 | INTRODUCTION

The interstitial pore space of the gravel substrate is crucial for fluvial geomorphology, the exchange processes between river and groundwater, and river ecosystems. Sediment transport studies have increasingly emphasized channel restoration and the quantification of environmental indices in response to natural or anthropogenic fine sediment pulses such as dam removal (Bednarek, 2001; Born et al., 1998; Cui et al., 2006; Cui & Wilcox, 2005; Doyle et al., 2003; Pollard & Reed, 2004; Stanley et al., 2002), dredge material disposal,

forest fires (Minshall et al., 2001; Vieira et al., 2004), watershed land use changes (Lisle, 1989; Swanson & Dyrness, 1975), and mining activities (Parker et al., 1996). Often, a large amount of fine sediment is flushed during dam removal operation, which is a standard practice to recover the reservoir capacity. Irrespective of the factors causing the fine sediment pulse, the infiltrated fine sediment results in the loss of the interstitial pore space in the gravel bed downstream. Therefore, predicting how the pore space varies in the gravel bed as a result of fine sediment infiltration could be of great importance in eco-hydraulic management and fine sediment budgeting.

While fine sediment might get infiltrated into the gravel bed through concurrent deposition of both fine sediment and coarse gravel. More often, fine sediment gets infiltrated into the static (immobile) gravel bed, especially in relatively low-flow conditions. The process of fine sediment infiltration into static gravel bed should be studied by distinguishing between two distinct infiltration processes, namely bridging and unimpeded static percolation, which result in loosely and densely packed gravel bed configurations, respectively. The distinction between bridging and unimpeded static percolation would be helpful to assess these processes, quantify their ecological impacts and accordingly take measures to prevent them. In bridging (or clogging) case, where fine sediment infiltrates only up to a limited depth, the majority of infiltrated fine sediment can be flushed by high flood events; thus, the gravel bed can be freed up from the infiltrated fine sediment. On the other hand, unimpeded static percolation results in deep entrainment of fine sediment. Hence, removing it from deeper layers of the gravel bed is difficult if not impossible. The schematic and experimentally observed unimpeded static percolation and bridging infiltration processes are shown in Figure 1 (Gibson et al., 2009). The process of fine sediment infiltration into static gravel bed has been intensively studied using physical experiments, theoretical and analytical models, and numerical simulations. However, the understanding of the process is still limited. Additionally, many contradicting observations were reported, as discussed in the following paragraphs.

One of the first studies on fine sediment infiltration into a static gravel bed, having a relatively shallow bed of thickness 1–2.7 times the coarsest gravel diameter, was conducted by Einstein (1968). Einstein observed the so-called unimpeded static percolation behaviour, where fine sediment first settles at the bottom of the gravel bed and gradually fills the interstices upwards. This behaviour was supported by other studies (Herrero et al., 2015; NCASI, 1981) and has also been documented in streams (Diplas & Parker, 1992; Evans & Wilcox, 2014; Lunt & Bridge, 2007). In contrast, the bridging (or clogging) type of infiltration process was observed (Beschta & Jackson, 1979; Carling, 1984; Frostick et al., 1984; Lisle, 1989; Schälchli, 1992), provided the gravel bed is thick enough. The bridging depth (or clogging depth) is approximately 2–5 times $d_{90,Gravel}$ (Beschta & Jackson, 1979; Diplas & Parker, 1992; Iseya & Ikeda, 1987). A stochastic model by Lauck (1991) reproduced both types of infiltration processes. His stochastic model is independent of how the fine sediment particles move downward within the gravel deposit framework (e.g., by gravity or intra-gravel flow), because lodging of the sediment particles is assumed solely a function of pore space geometry. With his model, he demonstrated that fine sediment fills the coarse sediment deposit from the bottom up when the size ratio of the bed material is large and the bed material is shallow. This was in support of observations that filling would occur from bottom to top onwards (unimpeded static percolation) if the gravel bed is shallow and fine sediment infiltrates only up to a finite depth (bridging or clogging) if the gravel bed is sufficiently thick. There is no clear specification in the literature regarding the gravel bed thickness, that is considered to be 'thick enough'. Here, we hypothesize (based on our results and previous research; discussed later on) that a gravel bed deeper than five times the coarsest gravel diameter can be considered as a thick bed.
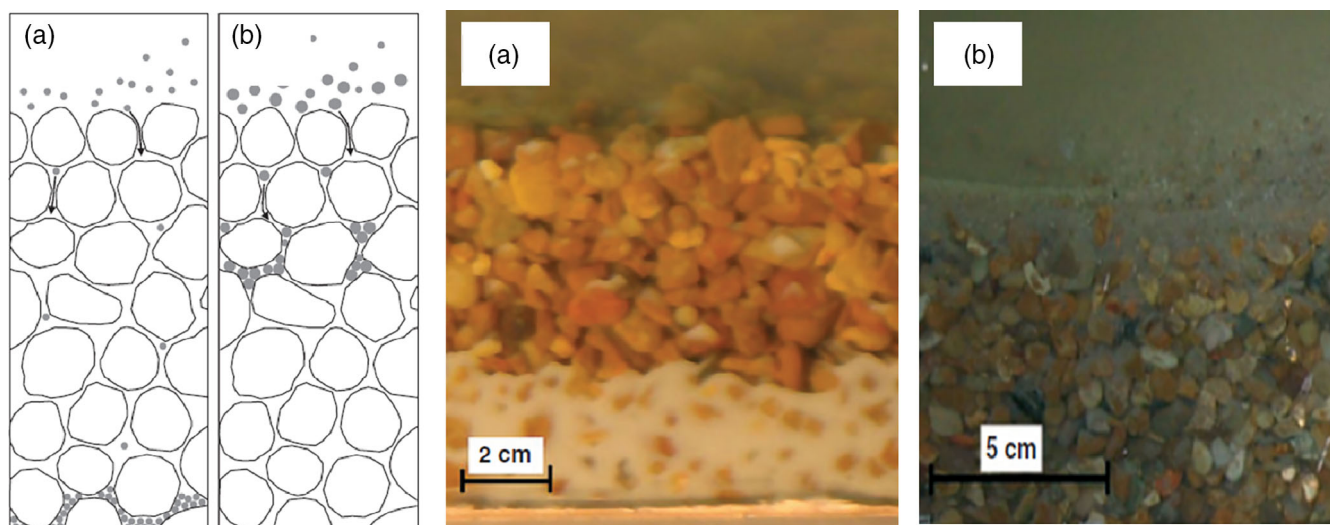
FIGURE 1 Schematic and experimentally observed (a) unimpeded static percolation and (b) bridging infiltration processes (Gibson et al., 2009). [Color figure can be viewed at wileyonlinelibrary.com]

Recently, Wooster et al. (2008) performed a set of flume experiments, where they observed only the bridging (or clogging) infiltration process into a static gravel bed, which was 8 times the coarsest gravel diameter deep (thick enough as per our hypothesis). They used different combinations of gravel and sand, whereby gravel ranged from 2 to 32 mm and sand had a geometric mean diameter of 0.35 mm and a standard deviation of 1.24. Cui et al. (2008) developed an analytical theory for the fine sediment infiltration into a static gravel bed and verified their theoretical model against experimental data from Wooster et al. (2008). They advocated that significant fine sediment infiltration occurs only up to a shallow depth (bridging or clogging behaviour), therefore fine sediment fraction follows an exponential decay function with the gravel bed depth. Interestingly, Gibson et al. (2009) observed both bridging and unimpeded static percolation behaviours within the same gravel bed, which was 10 times the coarsest gravel diameter deep (thick enough; thicker than the gravel bed considered in Wooster et al., 2008). This contradicts many previous observations, which claim that there will only be a bridging type of infiltration process, provided the gravel bed is thick enough. Gibson et al. (2009) related these two distinct infiltration processes to geotechnical filter theory. To quantify the gradation thresholds between these two processes, $d_{15,\text{Gravel}}$ is compared with $d_{85,\text{Fine Sediment}}$. For $d_{15,\text{Gravel}}/d_{85,\text{Fine Sediment}}$ ratios larger than 15.4, unimpeded static percolation, and for $d_{15,\text{Gravel}}/d_{85,\text{Fine Sediment}}$ ratios smaller than 10.6, bridging (or clogging) type of infiltration was observed. The size ratio for bridging (or clogging), observed in their experiment, is significantly higher than the theoretical and experimental geotechnical clogging criteria, which is normally 4–5. The standard filtering criteria used for filters in geotechnical engineering is thought by some to be a conservative design tool with inherent, undocumented safety factors (Kenney et al., 1985; Lone et al., 2005; Schuler & Brauns, 1993) and imprecise 'failure' criteria rather than theoretical process delineations. Sherard and Dunnigan (1989) put the process boundary at $d_{15,\text{Gravel}}/d_{85,\text{Fine Sediment}} = 9$, much closer to the boundary observed by Gibson et al. (2009). Due to the different particle size distributions (PSDs) of fine sediment and gravel used, different experimental setups and varying flow conditions in flume experiments, a straight-forward comparison is difficult. Claims have been made that only bridging type of infiltration occurs in nature (Beschta & Jackson, 1979; Carling, 1984; Cui et al., 2008; Frostick et al., 1984; Lisle, 1989; Schälchli, 1992; Wooster et al., 2008) and percolation is simply an artifact of shallow gravel bed (insufficiently thick gravel bed). Gibson et al. (2009) claim otherwise and advocate that bridging and unimpeded static percolation could occur within the same gravel deposit. Here, further studies should be done to solidify their observations and reach a unanimous conclusion concerning the occurrences of bridging and unimpeded static percolation.

More recently, a study by Huston (2014) used the literature-derived database to estimate the thresholds for bridging and unimpeded static percolation boundaries, combining 10 previously published studies, which included 146 data sets. They used median size ($d_{50,\text{Gravel}}$) and standard deviation (σ_{Gravel}) of gravel and median size ($d_{50,\text{Fine Sediment}}$) of fine sediment to represent bed-to-grain ratio. For $\frac{d_{50,\text{Gravel}}}{d_{50,\text{Fine Sediment}}\sigma_{\text{Gravel}}} > 27$ unimpeded static percolation and for $\frac{d_{50,\text{Gravel}}}{d_{50,\text{Fine Sediment}}\sigma_{\text{Gravel}}} < 27$ bridging behaviours were reported. The threshold suggested by Huston (2014) put the higher process boundaries than that of Gibson et al. (2009). Nevertheless, it is well-established and widely accepted that the size ratio of $d_{15,\text{Gravel}}/d_{85,\text{Fine Sediment}}$ remains the most reliable parameter to determine the process boundary (Honjo & Veneziano, 1989; Indraratna & Vafai, 1997; Sherard & Dunnigan, 1986), as the coarser portion of fine sediment and the finer portion of gravel are the important factors describing infiltration process (Indraratna & Locke, 1999). Huston (2014), based on regression analysis, suggested the bridging depth (or clogging depth) is positively correlated with gravel bed porosity and roughness Reynolds number, reflecting processes of gravity settling and turbulence-induced fluid pumping between gravel bed particles, respectively. On the other hand, Cui et al. (2008) suggested that the infiltration process is mainly gravity-dominated. Therefore, further investigation is necessary to conclude if gravity remains the most dominant factor governing the infiltration process.

Various theoretical and analytical packing models have also been developed and could be employed to understand the infiltration process. In this direction, theoretical models, originally developed to model interaction between base and filter materials in geotechnical engineering, introduced a term called 'controlling constriction size'. The controlling constriction size is defined as the largest base particle (fine sediment), which can pass through the filter (gravel bed). Considering the system of a binary mixture of spherical particles and the concept of controlling constriction size, the critical ratio of the entrance ($d_{\text{Fine Sediment}}/d_{\text{Gravel}}$) can be calculated based on idealized geometrical configurations. The theoretical critical ratio of entrance for dense (tetrahedra) and loose (cubic) packed beds are 0.154 and 0.414, respectively (Indraratna & Locke, 1999; Kenney et al., 1985). Some analytical packing models, mainly limited to binary and ternary mixtures of spherical particles, have also been developed (Yu et al., 1996). These models consider the geometrical packing limits to determine, how packing is formulated. The most popular packing models are linear and linear mixing packing models (Yu & Standish, 1991, 1993), where the critical ratio of the entrance is assumed to be 0.154, which corresponds to tetrahedral packing configuration. These analytical models are built upon the principle that for a given mono-sized particle assembly of spherical shape, there is an initial porosity ε_0 or initial specific volume $v_0 = 1/(1 - \varepsilon_0)$, which will decrease when particles of different sizes are added. With the addition of much smaller spheres, there is a regime of linear unmixing because the initial mono-sized particles retain their skeleton and simply have their gaps filled until the volume fraction of the added particles is sufficient to influence the skeleton. Alternatively, with the addition of marginally smaller particles, non-linear mixing occurs because the initial skeleton is disrupted to accommodate the additions. Modelling infiltration phenomena using these theoretical models, based on geometrical and analytical consideration, are indeed far from reality, but still could provide a fundamental basis for understanding infiltration mechanism. However, the infiltration process simulated with these models would still be lacking the effects of flowing water and turbulence, as these

models treat the system as a pure particle system. Here again, the question arises, to what extent these models can be applied to predict the infiltration process in fluvial deposits if it is hypothesized that fine sediment infiltration through intra-gravel flow is similar to fine sediment infiltration driven by gravity?

This hypothesis was first proposed by Cui et al. (2008). They developed an analytical theory to describe fine sediment infiltration into immobile gravel bed. The governing equations were derived from mass conservation with the assumption that fine sediment deposition per unit vertical distance into the deposit (trapping coefficient) is either constant or increases with fine sediment infiltration. The equations derived are similar to equations presented by Sakthivadivel and Einstein (1970), except for the equation for the trapping coefficient. Other than their claim that only bridging type of infiltration occurs in nature, they also hypothesized that fine sediment infiltration as a result of intra-gravel flow is similar to fine sediment infiltration driven by gravity. Similar assumptions were also made in Lauke's Stochastic model (Lauck, 1991), where the process is considered to be solely a function of pore space geometry, irrespective of how the fine sediment gets infiltrated into the gravel bed. Recently, a simple mathematical model (Herrero & Berni, 2016), based on Lauck's idea, could produce both bridging and unimpeded static percolation behaviours and verify Gibson et al.'s thresholds for their occurrences. However, this simple model also assumes the system to be a pure granular system and neglects the flowing water effects on the infiltration process. Further examination and validation are necessary to test the flowing water effects and Cui's hypothesis.

Modelling the mechanical behaviour of pure granular material using the discrete element method (DEM), first proposed by Cundall and Strack (1979), could also be adapted to simulate the infiltration processes. The DEM models can capture the realistic physical behaviour of particles, but consider the system to be pure granular media, that is, pure gravity-driven configuration. In this direction, Bui et al. (2019a, 2019b) have performed pure DEM simulations of the infiltration process, taking reference from the flume experiment conducted by Gibson et al. (2009). They were able to obtain quite good agreement with the experimental data, despite neglecting the effects of flowing water in their simulations. Although, it was not specifically mentioned in their papers, their observation has its roots in Cui's hypothesis. Nevertheless, the effects of flowing water on the infiltration process must be investigated to check the validity of the hypothesis. One can use computational fluid dynamics (CFD) to resolve the flow fields in greater detail and couple it with the DEM model to include the effect of flowing water. In this direction, we investigate the infiltration process by performing pure DEM and coupled CFD–DEM simulations. The coupled CFD–DEM method has various limitations concerning the number and the size of particles and is mainly categorized into two approaches, namely resolved and unresolved CFD–DEM. In the resolved approach, the fluid force acting on a particle can be calculated by integrating the fluid stress over the particle surface. For that purpose, a dense grid mesh is needed to obtain accurate fluid flow in CFD. Its applicability to particle-laden flow with a higher number of particles is limited due to the enormous

computational cost. The unresolved method uses empirical models, based on the relative velocity and porosity, to calculate fluid–particle interaction forces. Therefore, a dense grid is not necessary to obtain the fluid-particle interaction forces. The unresolved method allows relatively high computational efficiency for bulk particle-laden flows. More information on the CFD–DEM methods can be found in papers (Bérard et al., 2020; Kloss et al., 2012; Zhou et al., 2010).

It is evident that many contradicting observations concerning the infiltration process were reported and the process is still not entirely understood. The different behaviours (e.g., bridging and percolation) in the infiltration process seem to be independent of gravel bed thickness, rather their occurrences only depend on the relative size of fine sediment and gravel; thus, eventually on the formed pore space geometry and its connectivity. Physical experiments of these complex systems generally lack detailed information and are often very expensive and time-consuming. Therefore, numerical simulations, based on the physics involved, could be of great importance in understanding the infiltration process and assessing its ecological impacts. One can use the median gravel size ($d_{50,Gravel}$) to simplify the system (Indraratna & Locke, 1999). These simplifications might be necessary to apply statistical, theoretical, analytical, and numerical models to study the infiltration process. We model the infiltration process using the CFD–DEM approach, considering theoretical packing thresholds of the binary mixture, representing bridging and unimpeded static percolation. With the help of numerical simulations, we mainly aim to answer following two questions: (1) Can bridging and unimpeded static percolation occur within the same gravel bed, and if their occurrences are independent of gravel bed thickness? (2) Comparing the coupled CFD–DEM simulations with pure DEM simulations for several size ratios, we aim to validate Cui's hypothesis (Cui et al., 2008), which suggests that fine sediment infiltration through intra-gravel flow is similar to fine sediment infiltration driven by gravity.

2 | METHODOLOGY

We investigated the infiltration process with the help of numerical modelling. Here, the mechanical behaviours of particles is incorporated by employing DEM and fluid flow is resolved using CFD approach. More specifically, we use the unresolved CFD–DEM approach to model the infiltration process, where flow fields are obtained by solving Reynolds Averaged Navier–Stokes (RANS) equations, and particles are treated as discrete entities and tracked using Newton's second law of motion. Compared to single-phase (fluid) systems, the presence of particles modifies the fluid flow field in the two-phase (fluid–particle) systems. The RANS equations are accordingly modified to include the effects of particle fraction on fluid flow fields by including porosity and fluid–particle interaction term in governing equations. The CFD–DEM method is computationally demanding and has several limitations in terms of the number and size of particles (Bérard et al., 2020; Kloss et al., 2012). With currently available computational resources and infrastructure, the maximum number of particles, which can be simulated with the applied unresolved

CFD–DEM method, even in large clusters, is in the order of 10^7. Furthermore, the unresolved CFD–DEM method cannot be applied for cases, where particle size is greater than the CFD cell size, thus hindering mesh refinement, especially near walls that might be necessary for certain turbulence-resolving techniques. This restricts us to resolve flow fields at a relatively coarser scale.

2.1 | Fluid phase

Fluid flow is resolved by solving modified Navier Stokes (NS) equations numerically, which include the effect of particle's presence on the flow fields by including porosity, and fluid–particle momentum exchange forces as an additional source term in governing equations (CFD equations). There are mainly two different formulations, describing the fluid flow in the presence of particles, namely model A and model B (or BFull), which are originally derived from a continuum description of the two-phase system (Bérard et al., 2020; Zhou et al., 2010). The main difference between these different formulations is related to their treatment of the fluid–particle interaction forces in continuum and discrete descriptions. We used model A, which is more popular and also implemented in commercial software such as FLUENT and CFX (Zhou et al., 2010). The modified NS equations for fluid flow, considering 'model A' formulation, are:

$$\rho_f \left[\frac{\partial \varepsilon_f}{\partial t} + \nabla . (\varepsilon_f u) \right] = 0, \tag{1}$$

$$\rho_f \varepsilon_f \left[\frac{\partial u}{\partial t} + \nabla . (uu) \right] = -\varepsilon_f \nabla p - F_{pf}^A + \varepsilon_f \nabla . \tau + \rho_f \varepsilon_f g, \tag{2}$$

where, ρ_f is fluid density, $\varepsilon_f = (1 - \varepsilon_s)$ is porosity or volume fraction of fluid, ε_s is volume fraction of solid, u is the fluid flow velocity, p is fluid pressure, τ is fluid shear stress or deviatoric stress tensor, for Newtonian fluids $\tau = \mu \left[\nabla u + (\nabla u)^{-1} \right] - \frac{2}{3} \mu (\nabla . u) \delta_k$, g is acceleration due to gravity, F_{pf}^A is the fluid–particle interaction momentum exchange term, that includes drag force $f_{d,i}$ and other minor forces f_i'', if relevant in the system, such as virtual mass force f_{vm}, Basset force f_B, lift forces such as the Saffman force f_{saff}, and Magnus force f_{Mag}. One can see that pressure gradient and shear stress forces are not explicitly included in fluid–particle interaction term F_{pf}^A. Rather they are implicitly shared with the particle phase (solid phase), as seen in momentum equation where ∇p and $\nabla . \tau$ are multiplied by porosity. Therefore, the fluid–particle momentum exchange term can be written as:

$$F_{pf}^A = \frac{1}{\Delta V} \sum_{i=1}^{n} \left(f_{d,i} + f_i'' \right). \tag{3}$$

2.2 | Particle phase

Particles are described as discrete entities and tracked using Newton's second law of motion (DEM equations). The CFD–DEM approach is quite different than traditional two-fluid method (TFM), especially concerning the treatment of fluid–particle interaction terms in the particle phase. In the CFD–DEM approach, one has to consider the coupling between DEM at the particle scale and CFD at the computational cell scale. Using the soft-sphere approach, originally proposed by Cundall and Strack (1979), the translational and rotational motion of particle i with mass m_i, and moment of Inertia I_i, can be written as:

$$m_i \frac{dv_i}{dt} = f_{pf,i}^A + \sum_{j=1}^{k_c} \left(f_{n,ij} + f_{t,ij} \right) + m_i g, \tag{4}$$

$$I_i \frac{d\omega_i}{dt} = \sum_{j=1}^{k_c} \left(M_{t,ij} + M_{r,ij} \right), \tag{5}$$

where v_i and ω_i are translational and angular velocities of the particle i, k_c is the number of particles in interaction with the particle i. The forces involved are: the particle–fluid interaction force $f_{pf,i}^A$, the gravitational force $m_i g$ and inter-particle forces, which include the normal particle–particle contact force $f_{n,ij}$ and tangential particle–particle contact force $f_{t,ij}$. The torque acting on particle i by particle j includes two components: $M_{t,ij}$, generated by tangential force and $M_{r,ij}$, commonly known as the rolling friction torque and caused by non-sphericity of particle (not included, as we consider spherical particles). The fluid–particle interaction term f_{pf}^A, similar to F_{pf}^A in the continuum description (fluid phase), is the sum of all fluid–particle interaction forces acting on individual particles by fluid flow, including drag force f_d, pressure gradient force $f_{\nabla p}$, viscous force $f_{\nabla . \tau}$ due to fluid shear stress or deviatoric stress, and other usually not so relevant forces f'', such as virtual mass force f_{vm}, Basset force f_B, lift forces such as the Saffman force f_{saff}, and Magnus force f_{Mag}. Usually buoyancy force is included in the pressure gradient force. Therefore, the total particle–fluid interaction force acting on particle i can be written as:

$$f_{pf,i}^A = f_{d,i} + f_{\nabla p,i} + f_{\nabla . \tau,i} + f_i''. \tag{6}$$

Compared to the fluid phase description in the model A formulation, where the interaction term only includes $f_{d,i}$ and f_i''. In the solid phase description, the fluid–particle interaction term includes all the forces that can possibly act on particles by moving fluid. The additional forces (pressure gradient and viscous forces) contributing to the interaction term for the solid phase is due to an additional term, namely solid stress tensor, other than the fluid–stress tensor shared between fluid and solid phase, that appears while deriving the continuum description for the solid phase.

2.3 | Fluid–particle interaction forces

The momentum exchange term in the CFD and DEM sides have different forces in contribution as per model formulation considered (model A or model B), briefly touched upon in Sections 2.1 and 2.2. Both formulations are theoretically equivalent and describe the same physics (Bérard et al., 2020). In the fluid–particle interaction term, the relative importance of different forces mainly depends on the density ratio (specific gravity) and fluid–particle system under consideration.

For dense and heavy particles, drag force (f_d) contributes at the most (Armenio & Fiorotto, 2001) and in some scenarios pressure gradient ($f_{\nabla p}$) and viscous forces ($f_{\nabla.\tau}$) become also important. Other minor forces f'' come into picture, only when considering light particles (Kuerten, 2016) and unsteady flow (Bérard et al., 2020). For the considered system involving sand and gravel in flowing water, other minor forces f'' can be neglected. Therefore, drag, pressure gradient, and viscous forces are only considered in the fluid–particle interaction term. The general formulation of drag force on a single spherical particle is given by:

$$f_d = \frac{1}{2}\rho_f C_D A |u-v|(u-v), \tag{7}$$

where C_D is drag coefficient, A is area of sphere, and u and v are fluid and particle velocities, respectively. To characterize the drag force for multi-particle system, several models have been developed and nicely summarized in paper (Bérard et al., 2020). Initially, we tested several drag formulations for the considered case but they produced very similar results. Additionally, drag formulation of Koch and Hill (2001) seems to perform better for polydisperse particles and cover a broader range of Reynolds number. Considering this, we used the drag model developed by Koch and Hill (2001), which was implemented in following form:

$$f_d = f_0 + 0.5f_1 \operatorname{Re}_p, \tag{8}$$

$$f_0 = \begin{cases} \dfrac{1+3\sqrt{\dfrac{\varepsilon_s}{2}}+\dfrac{135}{64}\varepsilon_s \ln \varepsilon_s + 16.14\varepsilon_s}{1+0.681\varepsilon_s - 8.48\varepsilon_s^2 + 8.16\varepsilon_s^3} & \text{for } \varepsilon_s < 0.4 \\ 10\dfrac{\varepsilon_s}{(1-\varepsilon_s)^3} & \text{for } \varepsilon_s > 0.4 \end{cases}, \tag{9}$$

$$f_1 = 0.0673 + 0.212\varepsilon_s + 0.0232/(1-\varepsilon_s)^5, \tag{10}$$

$$Re_p = \frac{\varepsilon_f d_p |u-v|}{\vartheta}, \tag{11}$$

where ε_s is the solid fraction, ε_f is the void fraction or porosity, u is the fluid velocity at the location of particle, v is the particle velocity, d_p is the particle diameter, and ϑ is the kinematic viscosity.
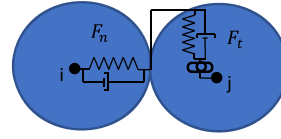
The forces due to pressure gradient and shear stresses are calculated using the following equations:

$$f_{\nabla p} = -V_p\left(\frac{\partial p}{\partial x}\right) = -\frac{1}{6}\pi d_p^3 \nabla P, \tag{12}$$

$$f_{\nabla.\tau} = V_p\left(\frac{\partial \tau_k}{\partial x_k}\right) = -\frac{1}{6}\pi d_p^3 \nabla.\tau. \tag{13}$$

2.4 | Particle–particle and particle–wall interaction forces

As shown in DEM equations, the particle's motion is due to the combined effects of gravity, fluid–particle interaction forces, and particle–

FIGURE 2 Simple spring-dashpot model. [Color figure can be viewed at wileyonlinelibrary.com]

particle contact forces. Particles' interaction with other particles (also with walls) is calculated based on the principle of the linear spring-dashpot model, usually known as the Hertz–Mindlin model (Johnson, 1987) shown in Figure 2. The total contact forces are calculated as the sum of the normal and tangential contact forces. The normal and tangential components of contact force are calculated based on the following equations:

$$f_n = -k_n \delta_n + c_n \Delta u_n, \tag{14}$$

$$f_t = \min\left\{\left|k_t \int_{tc,0}^{t} \Delta u_t dt + c_t \Delta u_t\right|, \mu f_n\right\}, \tag{15}$$

where Δu_n and Δu_t are the normal and tangential relative velocities of the particles in contact, respectively. k_n, k_t, c_n, and c_t are the normal and tangential spring and damping coefficients, which are functions of the overlap and depend on contact law implemented, either by linear or non-linear contact models, and δ_n is the normal overlap. The above formula also holds true for particle–wall contact. The integral term represents an incremental spring that stores energy from relative tangential motion, representing elastic tangential deformation of the particle surfaces that happened since the time when particle touched $t = t_{c,0}$. The second part, the dashpot, accounts for the energy dissipation of the tangential contact. The magnitude of the tangential force is truncated to fulfil the Coulomb friction limit with μ being the coefficient of friction, where the particles begin to slide over each other.

2.5 | Turbulence modelling

The CFD equations are presented in the form of full NS equations (Equations 1 and 2) modified for the two-phase systems. We used RANS equations to resolve the fluid flow fields. Due to Reynolds averaging, additional terms appear in momentum equations, called Reynolds stresses. The Reynolds stresses need to be calculated/modelled to close the RANS equations. One common approach is to calculate Reynolds stresses based on Boussinesq's hypotheses of eddy viscosity, which needs to be modelled. There are several models available to calculate the eddy viscosity, thus Reynolds stresses, such as kEpsilon, kOmega, kOmegaSST, and RNGkEpsilon, among many others. We have evaluated these turbulence models for our coupled CFD–DEM simulations in their ability to predict the flow and infiltration process.

It must be emphasized that the mathematical formulations of these turbulence models are developed based on studies on single

phase fluid flow and some works have noticed the potential failure of these turbulence models in specific flow scenarios (Gimenez et al., 2021). A straight-forward application of turbulence models, developed for single phase flow, to model two phase flow (fluid–particle) is probably not appropriate. However, new mathematical formulations for turbulence models considering the presence of particles are yet to be developed and do not come under the scope of this study.

2.6 | Numerical setup for pure DEM and coupled CFD–DEM simulations

All the simulations are performed with open-source CFD and DEM C ++ toolkits, namely OpenFOAM and LIGGGHTS, respectively. A separate CFDEM-Coupling code (Kloss et al., 2012) is deployed to couple the OpenFOAM and LIGGGHTS modules for coupled CFD–DEM simulations. The schematic of the applied unresolved CFD–DEM method is shown in Figure 3. The CFD (OpenFOAM) and DEM (LIGGGHTS) modules run sequentially and exchange data at a defined coupling interval. The DEM module initializes/updates the particle position, and the particle-related data such as diameter, position, and velocity are mapped onto CFD meshes. On the CFD side, fluid–particle interaction forces and porosity are calculated and averaged (volumetric) over each cell. Including the effects of fluid–particle interaction forces and porosity, NS equations are solved numerically. Newly obtained CFD flow fields such as velocity and pressure are transferred to the DEM side, where the new position and velocity of particles are calculated. This procedure is repeated till the specified run time.

Reference flume experiment (Gibson et al., 2009) was numerically simulated with the assumption that fine sediment and coarse gravel can be represented by spherical mono-size particles, representing a system of a binary mixture. Although due to this assumption, our simulations would not represent the exact gravel bed, void connectivity, and fine sediment infiltration as that of the original experiment. Yet, it should be able to provide enough information concerning the infiltration process and research questions, we aim to answer, as the assumptions made would not change involved physics. The geometry, particle and flow characteristics for pure DEM and coupled CFD–DEM simulations are summarized in Table 1. Flow conditions correspond to turbulent and subcritical flow, as Reynolds number and Froude number are (based on free surface velocity and water depth) 94,500 and 0.6, respectively. Three different size ratios of 0.154, 0.231, and 0.414 are chosen for both pure DEM and coupled CFD–DEM simulations. While size ratios of 0.154 and 0.414 correspond to tetrahedral (dense packing) and cubical (loose packing) geometrical packing configurations, respectively. The size ratio of 0.231 would represent a combination of both types of geometrical packing configurations. Median gravel size ($d_{50,Gravel} = 8$ mm) is chosen to represent the coarse gravel bed, and corresponding fine sediment size is calculated as 1.232, 1.848, and 3.312 mm for the size ratios of 0.154, 0.231, and 0.414, respectively. For our coupled CFD–DEM simulations, within the limitations of the unresolved CFD–DEM method, we obtain the open channel velocity profile (OCF) without resolving the interphase between air and water. The OCF is approximated using the symmetry boundary condition applied at the top boundary. This is a common CFD approach to model open channel flow without considering the air phase into the system.

The two main limitations of the unresolved CFD–DEM method, mentioned before, namely the number and size of particles, restricted us to resolve flow fields at relatively coarse scales (coarser than particle size) and also to reduce the domain size, which is significantly
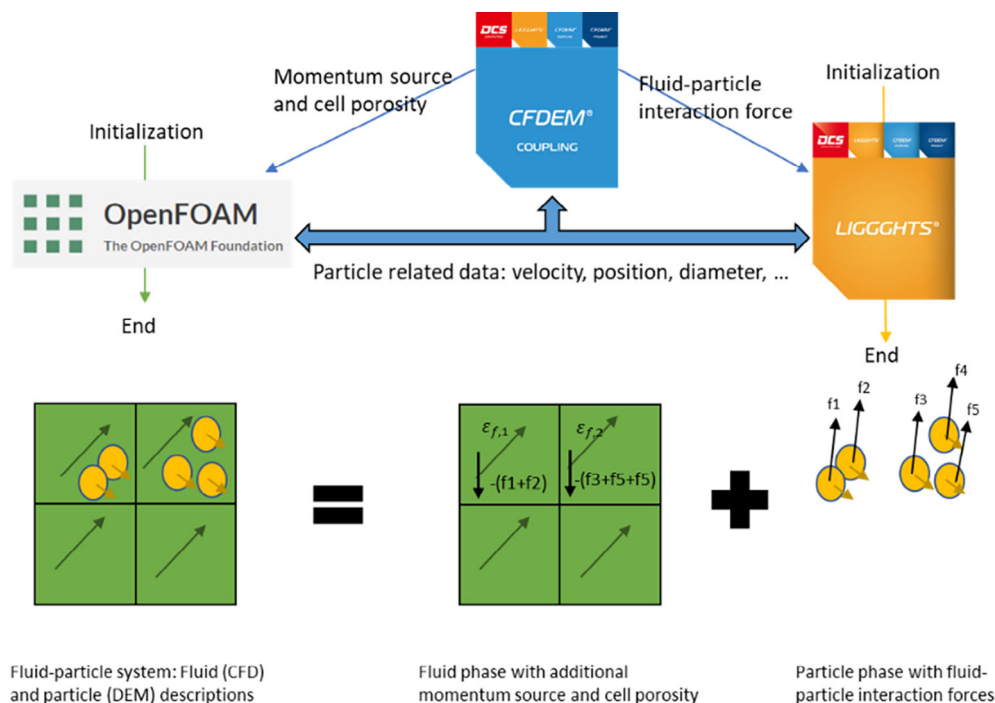
FIGURE 3 Schematic of unresolved CFD–DEM method implemented using OpenFOAM, LIGGGHTS and CFDEM-coupling modules. CFD, computational fluid dynamics; DEM, discrete element method. [Color figure can be viewed at wileyonlinelibrary.com]

TABLE 1 Geometry, particle and fluid flow characteristics for pure DEM and coupled CFD–DEM simulations.

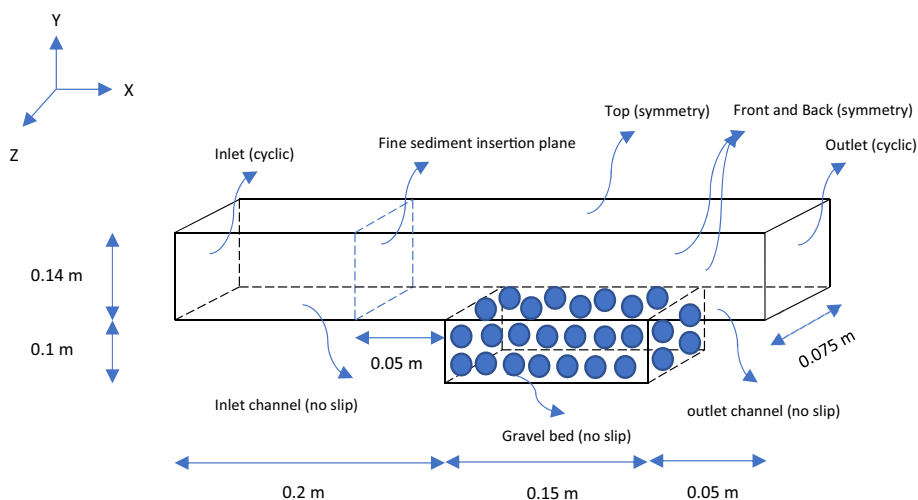|	Coupled CFD–DEM simulations	Pure DEM simulations
Geometry	Gravel bed length = 0.15 m	Gravel bed length = 0.15 m
	Gravel bed width = 0.075 m	Gravel bed width = 0.075 m
	Gravel bed height = 0.1 m	Gravel bed height = 0.1 m
	Inlet channel length = 0.2 m	Simulation box = $0.15 \times 0.2 \times 0.075$ m
	Channel width = 0.075 m	
	Outlet channel length = 0.05 m	
	Channel height (top boundary) = 0.14 m	
	Simulation box = $0.4 \times 0.26 \times 0.075$ m	
Particle (gravel and sand)	Young's modulus = 5×10^6 N/m^2	Young's modulus = 5×10^6 N/m^2
	Density = 2,700 kg/m^3	Density = 2,700 kg/m^3
	Poisson's ratio = 0.45	Poisson's ratio = 0.45
	Coefficient of restitution = 0.4	Coefficient of restitution = 0.4
	Coefficient of friction = 0.5	Coefficient of friction = 0.5
	Gravel diameter = 8 mm	Gravel diameter = 8 mm
	Sand diameter = 1.232, 1.848 and 3.312 mm	Sand diameter = 1.232, 1.848 and 3.312 mm
Fluid (water)	Mean flow velocity = 0.675 m/s	-
	Density = 1,000 kg/m^3	
	Kinematic viscosity = 1×10^{-6} m^2/s	
	Reynolds number = 94,500	
	Froude number = 0.6	

smaller than the actual flume experiment. The original flume experiment, adopted for our numerical simulations, was conducted in a 26 m long and 0.9 m wide flume, which would contain a much greater number of particles than the method's limitation concerning the maximum number of particles ($O \sim 10^7$). To overcome these limitations, we consider a reduced domain, which is 0.4 m long and 0.075 m wide for coupled CFD–DEM simulations, and 0.15 m long and 0.075 m wide for pure DEM simulations. In addition to the gravel bed region of the domain, extended inlet and outlet channels are provided in coupled CFD–DEM simulations to ensure that the flow is fully developed, before it reaches the gravel bed region. The extended inlet channel also serves the purpose of providing extra space required behind the insertion plane to generate and inject fine sediment. Although, reduced domain (length- and width-wise) is considered for numerical simulations, we keep the same gravel bed height (0.1 m) and water depth (0.14 m) as that of the original experiment. Different CFD mesh resolutions in the gravel bed and channel regions of the domain are used, ensuring that the particles are smaller than the CFD cell size in each part of the domain. In the channel section, much finer CFD mesh resolutions could be provided, as only fine sediment gets transported in this region of the domain, allowing us to resolve flow in much greater detail in the channel section. It must be noted that both pure DEM and coupled CFD–DEM simulations have the same size of the gravel bed region of a length of 0.15 m, a width of 0.075 m, and a height of 0.1 m. To inject fine sediment, an insertion plane is used,

which injects fine sediment at a specified mass flow rate for a specified duration. The insertion plane is located at 0.15 m downstream of the inlet because the desired insertion rate required some volume behind the insertion plane to generate and inject fine sediment. Due to the recirculation of flow and sediment from the outlet back to the inlet, and symmetry boundary conditions provided at the front and back planes, the effect of reduced domain size should vanish, and realistic flow and sediment transport in numerical simulations are expected, even with the reduced domain size. It must be emphasized that for pure DEM simulations, we have only considered the gravel bed region, and the fine sediment insertion plane is located above the gravel bed. Whereas, for coupled CFD–DEM simulations, the water flow enters through the inlet and fine sediment with desired mass flux is injected with an insertion plane located 0.15 m downstream of the inlet. Flow and fine sediment mass flux are linearly reduced for considered width of 0.075 m, which ensures that fine sediment and water flow are introduced at the same rate as that of the original experiment. The schematic diagram of the considered domain, with dimensions and boundary conditions, is shown in Figure 4.

Firstly, pure DEM simulations are performed for the size ratios of 0.154, 0.231, and 0.414. Pure DEM simulations would represent the infiltration process neglecting the flowing water effects. Keeping the same particle phase (DEM settings), the cases for each size ratio are modified to include the water flow and simulated with coupled CFD–DEM approach. All the simulations are performed with

224 processors (28-way Intel Haswell-based nodes and FDR14 Infiniband interconnect, 64 GB RAM per node) in a Linux cluster. For both pure DEM and coupled CFD–DEM simulations, the initial gravel bed is created with an initial bulk porosity of 0.454 by pouring gravel particles in the gravel bed region and then fine sediment is inserted at a specified mass flow rate with water flow (for coupled CFD–DEM simulations) or without the water (for pure DEM simulations). The selection of the initial porosity of the created mono-sized gravel bed is in accordance with previous pure DEM simulations (Bui et al., 2019a) and recommendations provided in the review paper (Latham et al., 2002). The mean water flow velocity of 0.675 m/s, the same as that of the original flume experiment, is provided and recirculated (cyclic boundary condition at the inlet and outlet). In the coupled CFD–DEM simulations, the extended inlet and outlet channels ensure fully developed turbulent flow at the inlet, and recirculation of flow and sediment as well. This also allowed us to dampen off the effects of reducing the domain size, as a reduced domain with recirculation would be equivalent to a sufficiently long flume (ideally infinite length).

Usually, DEM time steps are much smaller than CFD time steps to ensure stable solutions and realistic particle behaviour. Whereas, the stability on the CFD side is ensured by the Courant number criteria. On the DEM side, it rather depends on Rayleigh and Hertz time criteria. The DEM time step needs to be chosen sufficiently small to capture the phenomenon of energy transmission through wave propagation. Generally, it is sufficient to assume that all the energy is transmitted through Rayleigh waves. Hertz time step ensures that particles remain in contact sufficiently long enough to detect proper interaction among them. The Rayleigh and Hertz times depend on particle characteristics and materialistic properties. The DEM timestep is usually within 10%–20% of these times. The DEM and CFD time steps are selected following these criteria. The coupling interval is then calculated as the ratio of the CFD time step to the DEM time step. The CFD and DEM modules run sequentially and transfer data at defined coupling intervals. The simulation run times are 100 s for pure DEM simulations and the coupled CFD–DEM simulations are run till, either
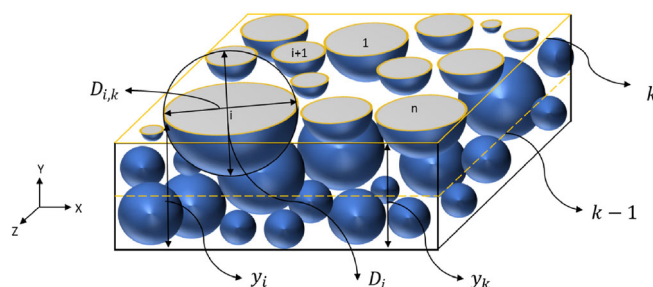
FIGURE 5 3D packing and circles generated cutting the packing by plane located at y_k. [Color figure can be viewed at wileyonlinelibrary.com]

the gravel bed is completely filled or fine sediment got trapped in the bed, obstructing further infiltration. Fine sediment is inserted at the mass flow rate of 0.01 kg/s for 80 s in pure DEM simulations and for 100 s in coupled CFD–DEM simulations, in total injecting 0.8 and 1 kg of fine sediment for pure DEM and coupled CFD–DEM simulations, respectively.

3 | RESULTS

To evaluate porosity and fine sediment fraction profiles along the depth of the gravel bed, a Matlab code has been written (Equations 16–19). The simulation results contain the 3-D packing information (demonstrated in Figure 5), such as the position and diameter of infiltrated fine sediment and gravel particles. The 3-D packing is cut at several planes across the depth (100 such planes have been generated for the results presented here), generating circles of different diameters at each cutting plane. With 100 planes cutting over 10 cm gravel bed depth, data are obtained for every 1 mm (smaller than the smallest particle in the system) from top to bottom of the bed. The area of generated circles is summed up at each cutting plane, representing the area of the solid fraction at the cutting plane.

Porosity (n) at the cut plane is calculated as the area of void divided by the total area (solid and void areas). The fine sediment fraction (f_s) at the cut plane is calculated as the area of fine sediment particles divided by the area of fine sediment and gravel particles. Although, our calculation of porosity and fine sediment fraction is based on the area instead of volume ratios, it represents the porosity and fine sediment fraction at each cut plane and would be required to evaluate, how the porosity and fine sediment fraction varies along the depth of the gravel bed.

$$D_{i,k} = \sqrt{D_i^2 - 4(y_k - y_i)^2} \text{ if } y_i - \frac{D_i}{2} \leq y_k < y_i + \frac{D_i}{2}, \tag{16}$$

$$A_{i,k} = \frac{\pi D_{i,k}^2}{4}, \tag{17}$$

$$n = \frac{A_k - \left\{ (\sum A_{i,k})_{\text{small}} + (\sum A_{i,k})_{\text{large}} \right\}}{A_k}, \tag{18}$$

$$f_s = \frac{(\sum A_{i,k})_{\text{small}}}{(\sum A_{i,k})_{\text{small}} + (\sum A_{i,k})_{\text{large}}}. \tag{19}$$

3.1 | Pure DEM simulations

By assuming that the process of fine sediment infiltration into static gravel bed can be described by a binary system of mono-sized spherical particles, theoretical packing limits based on different geometrical packing configurations are considered. The initial gravel bed and final infiltration state for the different size ratios after 100 s of simulation run time are shown in Figure 6. The size ratio of 0.154, which ideally represents the tetrahedral packing configuration, results in a densely
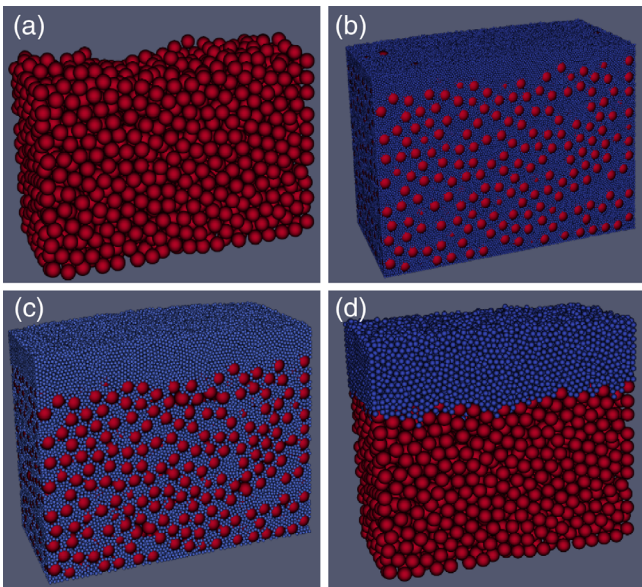
FIGURE 6 Initial gravel bed (a) and pure DEM simulated infiltration state at the end of simulation for size ratios of (b) 0.154, (c) 0.231 and (d) 0.414. DEM, discrete element method. [Color figure can be viewed at wileyonlinelibrary.com]

filled gravel bed. As expected for the size ratio of 0.154, fine sediment first settles at the bottom of the bed, and then filling occurs from bottom to top onwards, a so-called unimpeded static percolation is observed. For the size ratio of 0.414, which ideally represents cubical packing configuration, a so-called bridging behaviour is found, where fine sediment particles get clogged just below the gravel bed surface, precluding subsequent infiltration. A mixed behaviour is observed for the size ratio of 0.231, where some fine sediment particles are clogged in the gravel bed and some could reach the bottom of the gravel bed, representing simultaneous occurrence of both bridging and percolation infiltration processes. Fine sediment could also infiltrate to the bottom of the gravel bed for the size ratio of 0.231, but it generates a relatively less densely packed gravel bed, as compared to the size ratio of 0.154. The bulk porosity of the initially created gravel bed is 0.454 and it is reduced to 0.2166, 0.2879, and 0.4158 for size ratios 0.154, 0.231, and 0.414 after the infiltration process, respectively.

Figure 7 shows the detailed porosity (Figure 7a) and fine sediment fraction (Figure 7b) profiles along the gravel bed depth. One can see that a significant reduction in porosity is predicted for size ratios of 0.154 and 0.231. This reduction in porosity is almost uniform from the bottom to the top of the gravel bed, as fine sediment could infiltrate till the bottom of the gravel bed and filling could occur from bottom to top onwards. In contrast to this, the reduction in porosity is limited to the first 2 cm of the gravel bed for the size ratio of 0.414. After this depth, which is equivalent to 2.5 times the gravel diameter, no change in porosity is found. Fine sediment fraction profiles also support these behaviours for different size ratios. It can be seen that fine sediment first settles at the bottom and fills the voids upwards, for a size ratio of 0.154 and more or less for a size ratio of 0.231 as well. For a size ratio of 0.414, a bridging behaviour is observed and no fine sediment particle is found below 2 cm of the gravel bed surface. For the bridging case (size ratio 0.414), the maximum depth to which fine sediment could infiltrate is found to be ~2.5 times the gravel diameter, which aligns with the previously observed bridging depth (Beschta & Jackson, 1979; Diplas & Parker, 1992; Iseya & Ikeda, 1987). Small fluctuations in fine sediment fraction and porosity profile plots, along the gravel bed, might be due to our approach of considering porosity and fine sediment fraction as area average values, although porosity and fine sediment fraction are volume-based quantities. These fluctuations are more predominant at the bottom of the gravel bed, which might be due to wall effects and wall–particle interactions.

From Figures 6 and 7, it is also evident that different infiltration processes such as bridging, unimpeded static percolation, or a combination of both processes, could occur with the same gravel bed. In contrast to the consensus in the field, this observation suggests that the occurrences of bridging and percolation behaviours are independent of gravel bed thickness. We emphasize again that the gravel bed should be sufficiently thick enough to distinguish between these two different infiltration processes. It is still an open question: what depth of gravel bed is considered to be thick enough? Our hypothesized definition of a 'thick enough' gravel bed (thickness >5 times the coarsest gravel diameter) is reasonable and sufficient to distinguish between

these infiltration processes. The bridging depth is 2–5 times the $d_{90,Gravel}$, therefore the gravel bed needs to be thicker than this to make a distinction between different infiltration processes. Closely observing the porosity and fine sediment fraction profiles, one can see that if the depth of the gravel bed was less than the bridging depth (in our case, 2 cm or 2.5 times gravel diameter), one would have misinterpreted the bridging as a percolation process. Fine sediment could easily infiltrate till the bridging depth and one needs a thicker gravel bed to clearly see if further fine sediment infiltration beyond the bridging depth occurs or not. Although, our hypothesis seems reasonable, it is based on previously observed bridging depth (Beschta & Jackson, 1979; Diplas & Parker, 1992; Iseya & Ikeda, 1987) and our simulations on the simple case of constant bed thickness and mono-size spherical particles for gravel and fine sediment. A more thorough investigation might be necessary, where the bed size, a wide range of gravel and fine sediment, and non-sphericity should be considered, before our hypothesized definition of a 'thick enough' gravel bed is standardized.

3.2 | CFD–DEM simulations

To model the infiltration process with the coupled CFD–DEM approach, numerical simulations are performed in two stages. In the first stage, pure DEM simulations are performed to create the gravel bed with pre-defined porosity. In the second stage, CFD–DEM coupling is activated, where fine sediment particles are injected from the insertion plane at a desired mass flow rate and recirculated from the outlet to the inlet along with water flow. The simulation run times and required CPU times are summarized in Table 2, comparing them with their pure DEM counterparts. For smaller size ratios, it takes longer CPU time to reach the equilibrium infiltration state or steady-state condition (fine sediment is either clogged or has completely filled the gravel bed). The simulations for smaller size ratios are slower due to the increase in complexity and the number of calculations required, as a greater number of particles are required to represent the same mass for smaller size ratios. The CPU time increases several folds (at least ~6 times) with the inclusion of flowing water (CFD–DEM simulations). The coupled CFD–DEM simulations for larger size ratios are run for a longer duration, as they were relatively faster than that of smaller size ratios. The additional time required for coupled CFD–DEM simulations is due to extra computational effort in resolving fluid flow and the complexity associated with it.

The initial gravel bed and final infiltration states for different size ratios at the end of the simulation can be seen in Figure 8. The Infiltration processes simulated with the coupled CFD–DEM approach appear to be quite similar to their pure DEM counterparts. For the size ratio of 0.154, fine sediment first settles at the bottom of
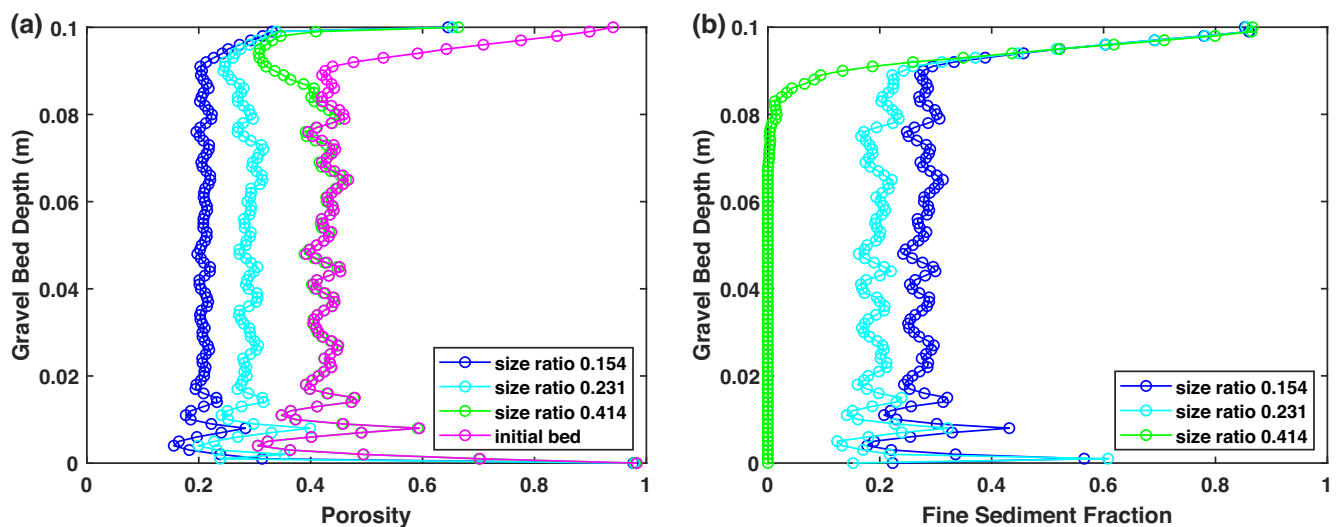

FIGURE 7 Variation of (a) porosity and (b) fine sediment fraction along the depth of gravel bed for different size ratios at the end of infiltration processes. [Color figure can be viewed at wileyonlinelibrary.com]

TABLE 2 Simulation run time and CPU time (or process time) for pure DEM and coupled CFD–DEM simulations.

| Size ratio | Pure DEM simulation | | Coupled CFD–DEM simulation | |
	Simulation run time (in seconds)	CPU time (in hours)	Simulation run time (in seconds)	CPU time (in hours)
0.154	100	8.89	176	96
0.231	100	3.36	195	48
0.414	100	0.98	200	13.5

Abbreviations: CFD, computational fluid dynamics; DEM, discrete element method; CPU, central processing unit.
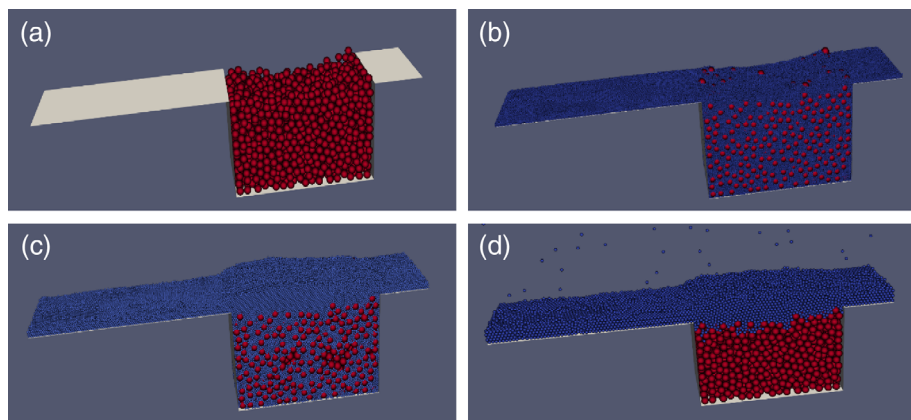
FIGURE 8 (a) Initial bed and coupled CFD–DEM simulated infiltration state at the end of simulation for size ratios (b) 0.154, (c) 0.231 and (d) 0.414. CFD, computational fluid dynamics; DEM, discrete element method. [Color figure can be viewed at wileyonlinelibrary.com]

TABLE 3 Initial and final porosity (after infiltration) for different size ratios.

|				Final porosity	
Size ratio	Gravel diameter (mm)	Fine sediment diameter (mm)	Initial porosity	Pure DEM simulation	Coupled CFD–DEM simulation
0.154	8	1.232	0.454	0.2166	0.2238
0.231	8	1.848	0.454	0.2879	0.2866
0.414	8	3.312	0.454	0.4158	0.4155

Abbreviations: CFD, computational fluid dynamics; DEM, discrete element method.

the gravel bed and fills the voids from bottom to top onwards, representing the unimpeded static percolation. For the size ratio of 0.414, fine sediment gets clogged just below the surface layer of the gravel bed, representing the bridging infiltration process. For the size ratio of 0.231, a combination of both types of infiltration processes is observed. The coupled CFD–DEM and pure DEM simulations, for all size ratios, predict similar infiltration processes and final infiltration states as well. The initial and final (after infiltration) bulk porosity of the gravel bed for coupled CFD–DEM simulations and pure DEM simulations are shown in Table 3. The final porosities of the gravel bed for coupled CFD–DEM simulations are 0.2238, 0.2866, and 0.4155 for size ratios of 0.154, 0.231, and 0.414, respectively. For smaller size ratios (0.154 and 0.231), very dense packing is generated and a significant reduction in porosity is predicted. This reduction in porosity is almost uniform along the depth of the gravel bed. On the other hand, for a higher size ratio (0.414), fine sediment gets clogged in the top surface layer below the gravel bed and an overall decrease in porosity is marginal. The final porosity values simulated with coupled CFD–DEM approach, for each size ratio, are in a similar range as that of final porosities simulated with pure DEM approach (see Table 3). The difference in simulated final porosity values for coupled CFD–DEM and pure DEM simulations are marginal and only 3%, 0.4%, and 0.07% for size ratios 0.154, 0.231, and 0.414, respectively. This demonstrates that fine sediment infiltration into static gravel bed seems to be independent of the factor causing the infiltration process, that is, fine sediment infiltration process is gravity-dominated.

The predicted bridging depth for coupled CFD–DEM simulation (bridging case; size ratio 0.414) is also 2 cm (or 2.5 times the gravel

diameter), exactly the same as predicted in pure DEM simulation. For the bridging case (size ratio 0.414), fine sediment could only infiltrate 2 cm in the gravel bed and this is true for both pure DEM and coupled CFD–DEM simulations. Predicting the same bridging depth, irrespective of the factor causing the infiltration process, again solidifies our observation that the infiltration process in fluvial deposits is gravity-dominated. Similar to pure DEM simulation, small fluctuations are also observed in the detailed porosity and fine sediment fraction profiles of our coupled CFD–DEM simulations. The probable reason for this fluctuating behaviour is already discussed in our previous pure DEM section.

The coupled CFD–DEM simulated porosity and fine sediment fraction profile plots for different size ratios, along with their pure DEM counterpart, can be seen in Figure 9. Figure 9a,c,e compare the coupled CFD–DEM simulated and pure DEM simulated porosity profiles for the size ratios of 0.154, 0.231, and 0.414, respectively. Figure 9b,d,f compare the coupled CFD–DEM simulated and pure DEM simulated fine sediment fraction profiles for the size ratios of 0.154, 0.231, and 0.414, respectively. It must be emphasized that the initial gravel beds used in pure DEM and coupled CFD–DEM simulations are not entirely the same and have a marginal variation in porosity and void connectivity, which can be seen in the initial porosity profile plots of the created gravel bed. This small difference in the initial gravel bed might be due to different wall treatments in pure DEM and coupled CFD–DEM simulations and consequently their effects on overall packing. To prepare the complex geometry in the coupled CFD–DEM simulation, STL files are considered as walls. Whereas, in pure DEM simulations simple rectangular box is considered by
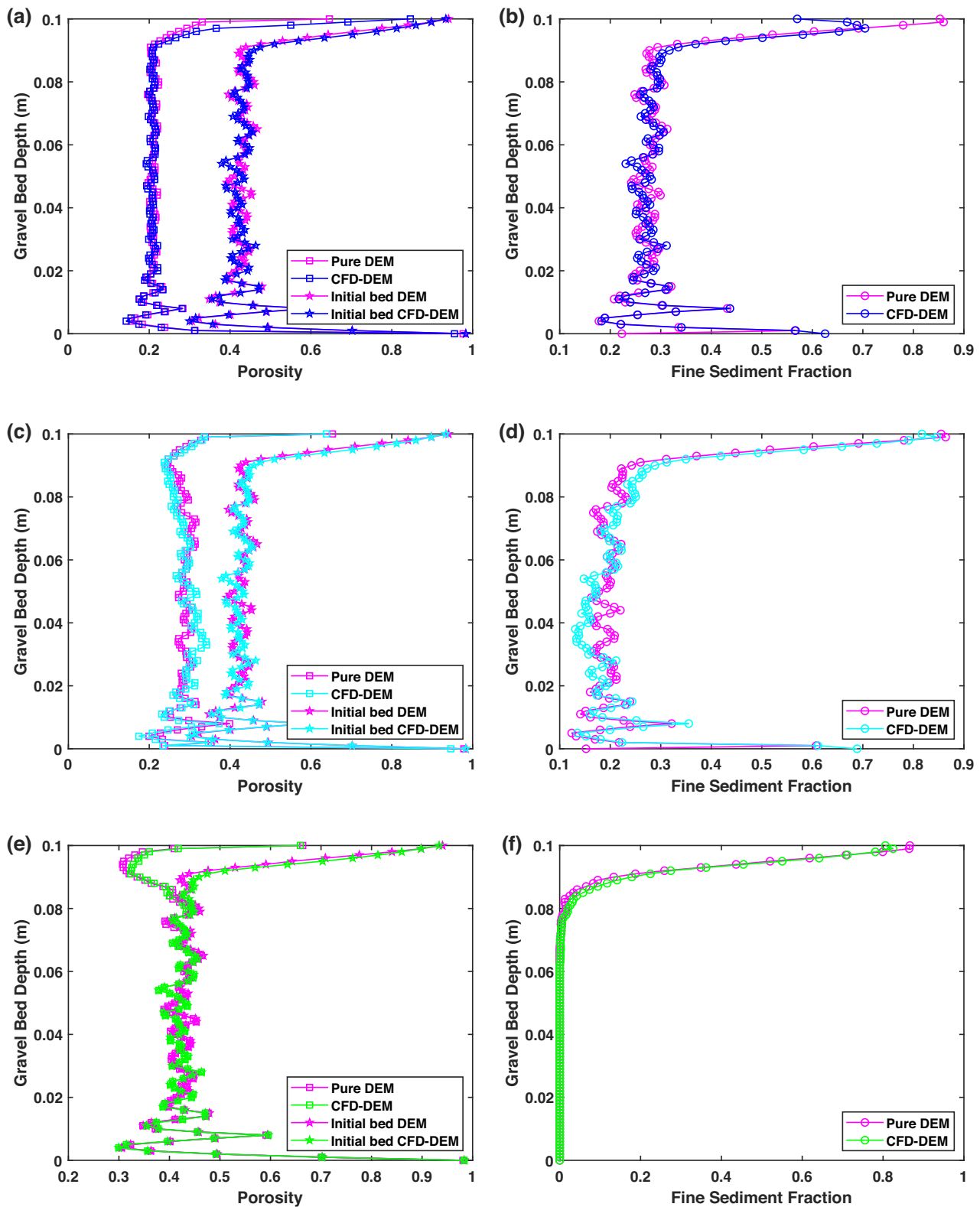
FIGURE 9 Comparison of coupled CFD–DEM simulated and pure DEM simulated infiltration processes in terms of porosity and fine sediment fraction for different size ratios. CFD, computational fluid dynamics; DEM, discrete element method. [Color figure can be viewed at wileyonlinelibrary.com]

treating planes as walls (no STL files). Additionally, the packing process is stochastic and might lead to small differences in created initial gravel beds, each time they are generated. Due to the marginal

difference in the created initial gravel bed, a small difference in coupled CFD–DEM and pure DEM simulated final infiltration state is expected but the bulk behaviours of the infiltration process should

not change. For the size ratio of 0.154 unimpeded static percolation, for the size ratio of 0.414 bridging, and for the size ratio of 0.231 a combination of both infiltration processes is observed and these behaviours are consistent for pure DEM and coupled CFD–DEM simulations. For the unimpeded static percolation case (size ratio 0.154), fine sediment first settles at the bottom and filling occurs from bottom to top onwards. For the bridging case (size ratio 0.414), fine sediment gets clogged near the bed surface and the maximum depth, they could infiltrate, is 2 cm, which is equivalent to 2.5 times of gravel diameter. The bridging depth of 2.5 times the gravel diameter aligns with the previous observations (Beschta & Jackson, 1979; Diplas & Parker, 1992; Iseya & Ikeda, 1987). As discussed in our pure DEM section, the gravel bed depth must be thicker than the bridging depth (usually 2–5 times $d_{90,Gravel}$), so that the different infiltration processes can be distinguished. Although, our hypothesized definition of 'thick enough' gravel bed seems reasonable and logical, a more thorough investigation using numerical simulations and flume experiments

might be necessary, where gravel bed depth, a wide range of gravel and fine sediment and non-sphericity of particles should also be addressed, before our hypothesized definition of 'thick enough' gravel bed is standardized.

3.3 | Effect of turbulence models on the infiltration process

We evaluate four different turbulence models, namely the kEpsilon, kOmega, RNGkEpsilon, and kOmegaSST model, in their ability to predict physical and realistic flow and infiltration process. For this purpose, we only consider the size ratio of 0.154 (unimpeded static percolation case). The streamwise mean (RANS resolved) and fluctuating velocity (modelled) profiles of water flow at the inlet, and porosity and fine sediment fraction profiles in the gravel bed region, for these turbulence models, are compared and summarized in Figure 10. It
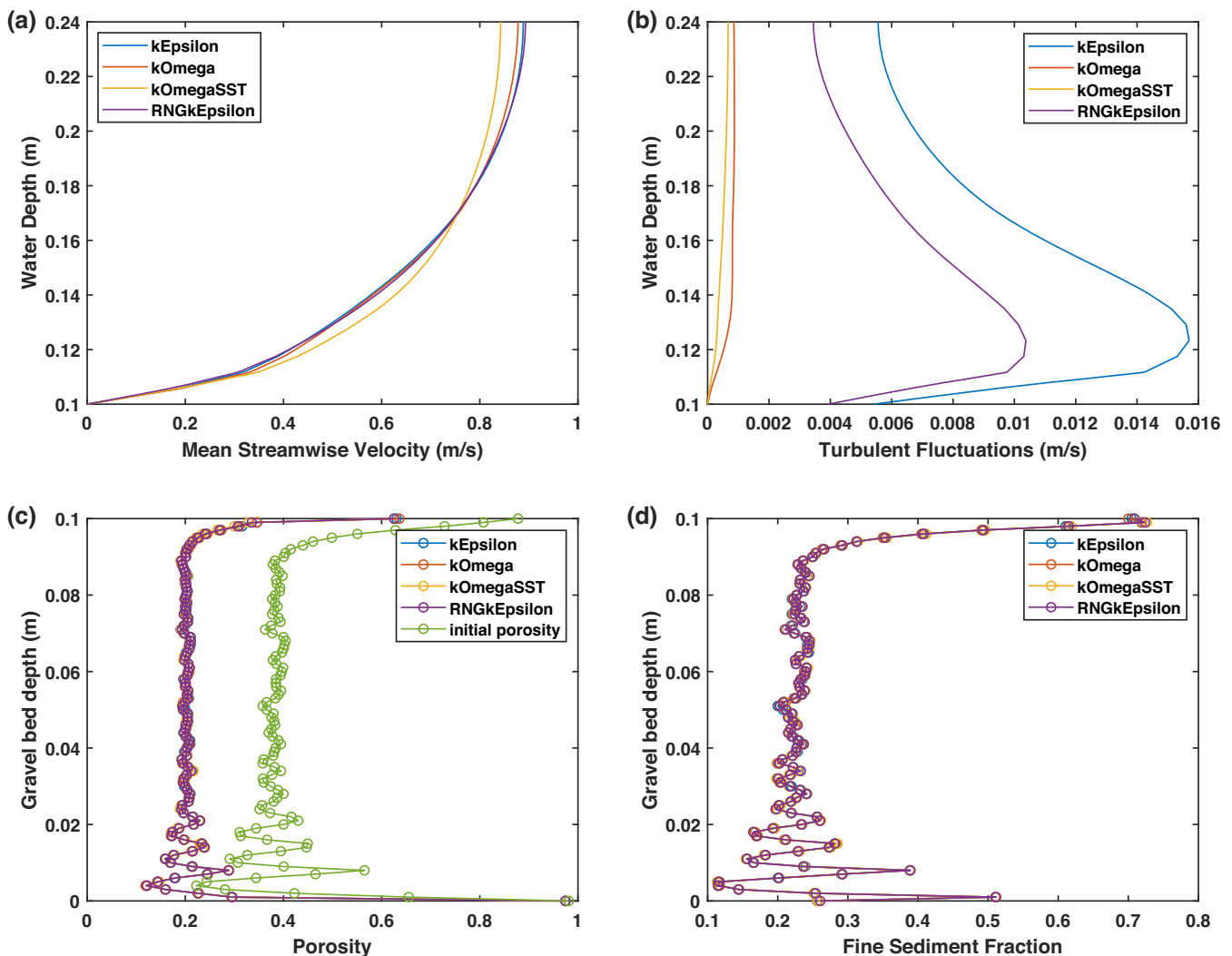
FIGURE 10 Comparison of RANS turbulence models in predicting (a) mean fluid velocity, (b) turbulent fluctuating velocity, (c) porosity and (d) fine sediment fraction profiles along the gravel bed depth. RANS, Reynolds Averaged Navier–Stokes. [Color figure can be viewed at wileyonlinelibrary.com]

must be emphasized that RANS resolves only up to mean flow statistics and the turbulent fluctuations are modelled using turbulence models by assuming the turbulence is isotropic in the whole domain. Turbulent fluctuations are simply calculated from modelled turbulent kinetic energy (k) as $u' = \sqrt{2k/3}$. Unfortunately, there were no detailed velocity profiles (both for mean flow and turbulent fluctuations) measured in the reference experiment. However, qualitative observation of the velocity profiles reveals that, all the RANS turbulence models, considered, are able to predict realistic mean fluid velocity profiles (Figure 10a). Omega-based models predict small and physically realistic turbulent fluctuations, whereas Epsilon-based models predict large turbulent fluctuations (Figure 10b). As seen in Figure 10c,d, there is hardly any difference in predicted final porosity and fine sediment fraction profiles, for the turbulence models considered. It can be seen that the final porosity and fine sediment fraction profiles, for all the turbulence models, are overlapping. This is due to the fact that only mean flow statistics are used to calculate fluid's effect on particle motion. As long as the mean flow fields are accurately captured by the turbulence model used, similar infiltration processes will be predicted irrespective of the turbulence model. However, this approach can only be applied for low-flow conditions, where the gravel bed remains static and fine sediment simply get transported over the gravel bed. The comparison of our pure DEM and coupled CFD–DEM simulations, for different size ratios considered, advocates that the process of fine sediment infiltration into static gravel bed is mainly gravity-dominated. Therefore, one may simply neglect the effect of turbulent fluctuations on the infiltration process. In high-flow conditions, to predict accurate and physically realistic sediment transport, a proper evaluation of turbulence fluctuations might be important and should be included by some additional models such as Stochastic dispersion models (Minier et al., 2014). Our results on different turbulence models demonstrate that for the low-flow conditions, where the process of fine sediment infiltration into the immobile gravel bed seems to be gravity-dominated, any of the turbulence models can be applied as long as it is able to capture mean flow statistics properly.

From Figure 10c,d, it can be seen that large predictions of turbulent fluctuations are not propagated to the infiltration process. Final porosity and fine sediment fraction profiles are overlapping for all the turbulence models considered. In the unresolved CFD–DEM method, the forces acting on particles, due to fluid flow, are calculated using empirical equations, mostly based on mean flow statistics. In a broader sense, the information on the fluid velocity at the particle's position (fluid velocity seen by particles) is used to calculate fluid–particle interaction forces (see Section 2.3). The more precisely flow fields are resolved, the more accurate estimation of the interaction forces is expected, thus more physical particle's trajectory is predicted. For example, direct numerical simulation (DNS) and large-eddy simulation (LES) in conjunction with DEM could be alternative approaches. As DNS and LES resolve flow beyond mean flow fields and eventually would result in a more accurate estimation of fluid–particle interaction terms. The DNS–DEM or LES–DEM is mostly not possible, especially for particles larger than typically resolved flow fields (Jaiswal et al., 2022). One has to compromise with the coarsely resolved flow

fields, such as mean flow fields, resolved with the RANS approach, especially dealing with large particles such as gravel and sand. The RANS–DEM approach neglects the effects of turbulent fluctuations on the particle's trajectory and additional dispersion models would be required to recover the lost turbulent fluctuations due to RANS averaging (Bocksell & Loth, 2006; Jaiswal et al., 2022; Loth, 2000; Minier et al., 2014). However, the inclusion of the dispersion model should be decided based on the process under consideration and might not be necessary. It might be sufficient to include only mean flow statistics, yet able to capture realistic particle behaviour in a turbulent flow. In many physical processes, especially disperse-particle flow, it might be necessary to include the effect of turbulent fluctuations on particle motion. As our results demonstrated that the process of fine sediment infiltration into static gravel bed is mainly gravity dominant process, therefore the inclusion of additional dispersion models might not be necessary. We expect that the effects of turbulent fluctuations can only be neglected in low-flow conditions. As soon as the gravel particle starts to move, it cannot be simply assumed as a gravity-dominated process and under those scenarios, one should include the effect of turbulent fluctuations using dispersion models.

Among the two main factors (gravity and turbulence) describing the infiltration process, suggested by Huston (2014), an eddy-resolving approach could be applied to assess the turbulence effect on infiltration in greater detail. This can be achieved by employing a more detailed approach 'resolved CFD–DEM' to model the infiltration process. The eddy generation and dissipation process can be properly captured by DNS thus turbulence effects on the infiltration process can be in detail investigated. The resolved CFD–DEM method calculates interaction forces acting on particles (i.e., fluid–particle interaction force) by integrating fluid stresses on the surface of particles, rather than empirical models used in unresolved CFD–DEM. However, it requires enormous computational resources and is limited to the maximum order of 10^3 particles (Bérard et al., 2020; Kloss et al., 2012). Due to the small number of particles in resolved CFD–DEM method, the resolved CFD–DEM approach might not be appropriate to model and capture the bulk behaviour of large systems, such as fine sediment infiltration into gravel bed.

4 | DISCUSSION

From both pure DEM and coupled CFD–DEM simulations, it is evident that the claims made in several previous studies that only bridging type of infiltration process occurs in nature and fine sediment infiltrate only till limited depth and percolation is simply an artifact of the shallow gravel bed, is not true. As shown in our both pure DEM and coupled CFD–DEM simulations, both infiltration processes, sometimes a combination of both, could occur within the same gravel bed. The occurrence of bridging and percolation mainly depends on the relative size of fine sediment and gravel; in a broader sense it depends on relative grain size distributions of fine sediment and gravel. Gravel grain size distribution determines the size of voids formed and eventually the smallest size of fine sediment, which could pass through

it. Fine sediment distribution eventually decides if the packing (or infiltration) could occur by bridging or percolation mechanism. Based on our results, we advocate that it is the relative size ratio of fine sediment and gravel that ultimately determines, which type of infiltration would occur.

Furthermore, our results for pure DEM and coupled CFD–DEM simulations, for different size ratios, suggest that the infiltration process is gravity-dominated. Considering a realistic scenario of gravel beds in natural streams. Usually, there exists low permeable or impermeable strata below the gravel bed. This implies that there is an insignificant amount of downward flux (almost zero flow) along the direction of the bed depth due to the impermeable surface below the gravel bed in natural streams. Flume experiments are mostly aimed to model fluvial processes occurring in natural streams neglecting surface-ground water exchange. Our CFD–DEM setup is a representation of the infiltration process occurring in the flumes and natural streams, below which there exists an impermeable stratum. The hypothesis (Cui et al., 2008), suggesting that the process of fine sediment infiltration through intra-gravel flow is similar to the infiltration process driven by gravity, seems to be reasonable, even in scenarios, when there is a downward flux (flow along the gravel bed depth). We expect that the bridging and percolation should still be predominantly a function of pore space geometry and its connectivity. Even, when there is a downward flow (due to the permeable surface beneath the gravel bed, also called intra-gravel flow), it cannot push the fine particle further downward (if pore space is smaller than particle size), unless the gravel bed is mobilized. This argument strongly indicates that Cui's hypothesis might be valid even when there is downward flux. It must be emphasized that this hypothesis does not hold true for high-flow conditions, when the gravel bed becomes dynamic and mobile. As soon as the gravel particles in the bed start to move, which would typically be expected in high-flow conditions, the infiltration processes can no longer be simulated as a gravity-driven configuration and the water flow and turbulence effects must be included in the numerical simulations. However, as long as the gravel bed remains immobile, typically in low-flow conditions, one can simply simulate the infiltration process considering the system as pure granular media and yet able to predict realistic infiltration processes with much lesser computational resources and time, as shown by our pure DEM and coupled CFD–DEM simulations. However, this can be further investigated and verified by making the surface below the gravel bed permeable in coupled CFD–DEM simulations.

Our hypothesized definition of a 'thick enough' gravel bed (thicker than five times the coarsest gravel diameter) seems to be reasonable, as the maximum bridging depth is 2–5 times the $d_{90,Gravel}$. One would need a thicker gravel bed to distinguish between the bridging and percolation behaviours. In our case, the gravel bed thickness is 10 times the gravel bed diameter (sufficiently thick). We could simulate both types of infiltration processes within the same bed thickness. This demonstrates that bridging and percolation infiltration processes could occur in the same gravel bed and it mainly depends on the size ratios of considered fine sediment and gravel, rather than the gravel bed thickness.

One question that should be addressed here is: if both percolation and bridging could occur within the same depth of the gravel bed, which is thick enough, then why did Wooster et al. (2008) observe only bridging (or clogging) behaviour, despite using various combinations of gravel and fine sediment in their flume experiment? This hints towards the possibility that the materials, used in their experiment, might coincidently fall below the threshold for the bridging ($d_{15,Gravel}/d_{85,Fine\ Sediment} < 10.6$). To check for this possibility, we analyzed the data presented in their paper against the size ratio thresholds for bridging and percolation of Gibson et al. (2009). The $d_{15,Gravel}$ for different zones (different locations in flume) is directly extracted from the gradation curves provided in their paper. Unfortunately, for the fine sediment, only geometric mean (D_g) and standard deviation (σ_g) were reported in their paper, rather than a full gradation curve. Often, natural sediments follow a log-normal distribution and $d_{84.1}$ ($\sim d_{85}$) and $d_{15.9}$ ($\sim d_{15}$) can be approximated (Sundar & Sannasiraj, 2019) with geometric mean (D_g) and standard deviation (σ_g). Assuming fine sediment, used in Wooster et al.'s flume experiment, follow a log-normal distribution, a simple model is used to approximate the $d_{85,Fine\ Sediment}$, using the following relation:

$$Dg = (d_{84.1}d_{15.9})^{1/2}, \quad (20)$$

$$\sigma g = \log\left(\frac{d_{84.1}}{d_{15.9}}\right)^{1/2}. \quad (21)$$

We analyze the dataset presented in their paper and our approximated $d_{15,Gravel}/d_{85,Fine\ Sediment}$ for each zone can be seen in Figure 11. Almost all combinations of fine sediment and gravel used in their experiment lie below the size ratio threshold for bridging ($d_{15,Gravel}/d_{85,Fine\ Sediment} < 10.6$), except one section (Zone 4; refer to their paper for details). In Zone 4, the approximated $d_{15,Gravel}/d_{85,}$
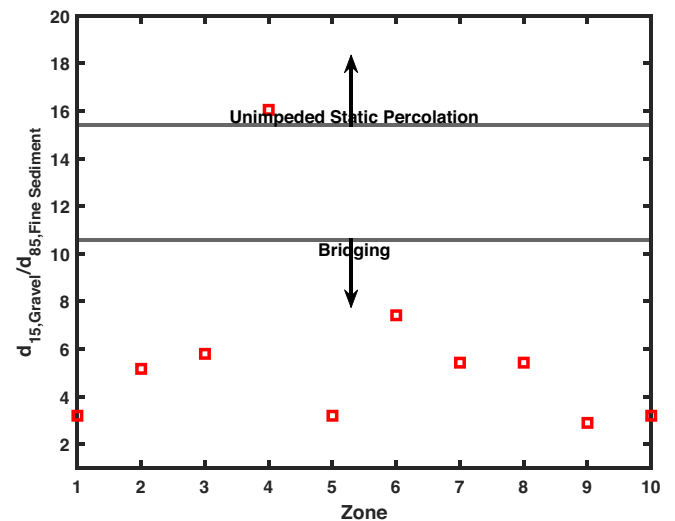
FIGURE 11 $d_{15,Gravel}/d_{85,Fine\ Sediment}$ for each zone in flume experiment of Wooster et al. (2008). [Color figure can be viewed at wileyonlinelibrary.com]

$_{Fine\ Sediment}$ is found to be 16 (near 15.4; percolation limit). Being at the border of bridging and percolation limits, the combination of bridging and percolation should have occurred in Zone 4. As the experiment was stopped by visual observation by looking through the glass walls of the flume, when the top surface layers of the whole flume (almost all zones) were clogged with fine sediments. Zone 4 might have remained unsaturated by the time the flume experiment was stopped. This section of the flume (Zone 4) could have shown the percolation behaviour (or combination of bridging and percolation) if the flume experiment would have run for a longer duration. As the size ratios, for most of the fine sediment and gravel combinations used in their experiment, corresponded to the bridging process, they observed only the bridging type of infiltration. Second, their observation of bridging behaviour in Zone 4 might be also due to different equilibrium fine sediment transport rates upstream and downstream of Zone 4. As different gravel sizes were used in each zone, they would be requiring different equilibrium fine sediment rates. This would affect the fine sediment transport process in other zones, depending on if the upstream or downstream section (zone) has more or less transport capacity than fine sediment entering that zone. One would have to run the experiment for a sufficiently long duration to make sure that the effects of different equilibrium fine sediment transport in different zones are vanished. The above discussion hints that Wooster's observation of only the bridging infiltration process, in their flume experiment, might be due to (a) the most of gravel and fine sediment material lying below the threshold for the bridging process, and (b) the short run-time of the flume experiment.

Another limitation, of not only the applied unresolved CFD–DEM method but also in general of the CFD–DEM method, is its inability to resolve fluid-air interphase. While, modelling systems involving multi-phases such as open channel flow with sediment transport (air, water, and particle), it might be important to capture the dynamics of the free surface. This would require the extension of the applied CFD–DEM method by coupling it with some interphase resolving methods, such as the level set method or volume of fluid method (VOF) (Harikrishnan & Mahapatra, 2021; Nan et al., 2023; Washino et al., 2023). However, the infiltration process occurs far from the free surface, as fine sediment infiltrates into the gravel bed as a result of bed load transport. Therefore, resolving the interphase between air and water (free surface) should not be causing any significant change in modelling infiltration processes and the final state of infiltration.

Furthermore, we have considered only spherical particles in our simulations but natural sediment particles have non-spherical shapes. Non-spherical particles behave much differently than spherical particles and particle shape could have significant effects on fluid–particle interactions and resultant particle movement (Washino et al., 2023). Additionally, natural sediment consists of various grain size distributions (non-uniform/polydisperse particles). We expect that a more realistic and accurate infiltration process could be obtained with numerical simulations by considering the non-sphericity and non-uniformity of particles into account.

5 | CONCLUSION

The process of fine sediment infiltration into static gravel bed is investigated by means of numerical simulation, where the mechanical behaviour of particles is considered using the DEM and fluid flow (water) is resolved using CFD. Due to various limitations of the applied unresolved CFD–DEM method, concerning the number and size of particles, and computational requirements, a smaller domain size, with monodisperse spherical particles for gravel and fine sediment, is considered. Two separate sets of simulations, namely pure DEM and coupled CFD–DEM simulations, are performed. Numerical simulations are based on the assumption that the process of fine sediment infiltration into a static gravel bed can be represented by a binary mixture of mono-sized spherical particles. Theoretical packing limits corresponding to the different geometrical configurations are considered for both sets of simulations. Taken together, the following conclusions can be drawn from the conducted study:

- The pure DEM (neglecting water flow) and coupled CFD–DEM (considering water flow) simulations of fine sediment infiltration into static gravel bed demonstrate that the process seems to be gravity-dominated. Our results and discussion advocates for Cui's hypothesis that fine sediment infiltration through intra-gravel flow is similar to fine sediment infiltration driven by gravity. This implies that the process could simply be simulated and studied using models developed for pure particle systems, such as stochastic models, analytical packing models, and also pure DEM simulations. However, this holds true for low-flow conditions, where the gravel bed remains immobile (static). As soon as gravel starts to move, the process cannot be modelled with pure particle models and flowing water and turbulence effects must be included.

- In contrast to the consensus in the field, we could able to simulate both bridging and percolation types of infiltration processes within the same gravel bed. For the size ratio of 0.154, 0.414, and 0.231, unimpeded static percolation, bridging, and a combination of bridging and percolation are observed, respectively. This shows that the occurrence of bridging and percolation processes are independent of gravel bed thickness, rather it only depends on the relative grain size distribution of fine sediment and gravel (size ratio).

- A sufficient thick gravel bed is necessary to distinguish between bridging and percolation behaviours. Based on our predictions and previous observations of bridging depths, we hypothesize that a gravel bed deeper than five times the coarsest gravel diameter can be considered as a thick bed. Although, our hypothesis seems reasonable, a more thorough investigation is required considering different gravel bed depths, detailed grain size distributions (polydisperse particles) and non-sphericity of particles, before our hypothesis is standardized.

- Previous claims that there is only a bridging type of infiltration occurs in nature and percolation behaviour is simply an artifact of the shallow gravel bed, supported also by recent studies of Cui et al. (2008) and Wooster et al. (2008), are not true. Our analysis indicates that almost all gravel-fine sediment combinations used in

their experiment lie below the bridging threshold. Additionally, their observations might also be due to the short run-time of the flume experiment.

- As long as the mean flow fields are correctly captured and the gravel bed remains immobile, the turbulence models seem not to affect the final state of infiltration. This also indicates that the fine sediment infiltration into static gravel bed is a predominantly gravity-driven process. However, our simulations are based on fluid–particle interaction forces, which do not consider the effect of turbulent fluctuations into account. It might be interesting to include the effects of the turbulent fluctuations either by simple dispersion models or by turbulence-resolving methods (resolved CFD–DEM) and simulate the infiltration process. This would solidify our observations that fine sediment infiltration is in-fact gravity dominant.

We have restricted ourselves to mono-disperse (uniform) gravel and fine sediment, due to computational and time restrictions. It might be interesting and helpful to include polydisperse (non-uniform) gravel and fine sediment with varying flow conditions, different gravel bed depths, and possibly the non-sphericity of particles. Turbulence-resolving approaches (resolved CFD–DEM) would provide more detailed insights into flow and infiltration processes occurring through the gravel bed. The resolved CFD–DEM approach would be helpful to assess the effects of turbulence on the infiltration process and clogging depth by directly resolving the phenomena of production and dissipation of turbulent eddies. As mentioned before, the resolved CFD–DEM approach is probably not a suitable approach to model the infiltration process, due to its limitation concerning a very limited number of particles and heavy computational requirements. Despite several simplifications and assumptions made to model the infiltration process, results obtained in the current study with unresolved CFD–DEM method, are indeed able to fill some research gaps in the overall understanding of the infiltration mechanism. A more detailed study, considering larger domain size and actual grain size distributions of fine sediment and gravel, would be helpful to solidify our conclusions. However, the applied unresolved CFD–DEM method (or CFD–DEM method in general) is computationally demanding and limited to a definite number of particles. With a large number of particles and varying PSD, the computational requirement will increase exponentially. This would be very difficult with currently available computer architecture, solution, and coupling algorithm and without proper and efficient parallelization (MPI load balancing). GPU-based codes for CFD–DEM coupling will also be helpful to simulate the process in realistic timeframes.

CONFLICT OF INTEREST STATEMENT

On behalf of all authors, the corresponding author states that there is no conflict of interest.

DATA AVAILABILITY STATEMENT

The data that support the findings of this study are available from the corresponding author upon reasonable request.

ORCID

Atul Jaiswal https://orcid.org/0000-0003-0228-5778

REFERENCES

Armenio, V., & Fiorotto, V. (2001). The importance of the forces acting on particles in turbulent flows. *Physics of Fluids*, *13*(8), 2437–2440. https://doi.org/10.1063/1.1385390

Bednarek, A. T. (2001). Undamming rivers: A review of the ecological impacts of dam removal. *Environmental Management*, *27*(6), 803–814. https://doi.org/10.1007/s002670010189

Bérard, A., Patience, G. S., & Blais, B. (2020). Experimental methods in chemical engineering: Unresolved CFD–DEM. *The Canadian Journal of Chemical Engineering*, *98*(2), 424–440. https://doi.org/10.1002/cjce.23686

Beschta, R. L., & Jackson, W. L. (1979). The intrusion of fine sediments into a stable gravel bed. *Journal of the Fisheries Research Board of Canada*, *36*(2), 204–210. https://doi.org/10.1139/f79-030

Bocksell, T. L., & Loth, E. (2006). Stochastic modeling of particle diffusion in a turbulent boundary layer. *International Journal of Multiphase Flow*, *32*(10–11), 1234–1253. https://doi.org/10.1016/j.ijmultiphaseflow.2006.05.013

Born, S. M., Genskow, K. D., Filbert, T. L., Hernandez-Mora, N., Keefer, M. L., & White, K. A. (1998). Socioeconomic and institutional dimensions of dam removals: The Wisconsin experience. *Environmental Management*, *22*(3), 359–370. https://doi.org/10.1007/s002679900111

Bui, V. H., Bui, M. D., & Rutschmann, P. (2019a). Advanced numerical modeling of sediment transport in gravel-bed Rivers. *Water*, *11*(3), 550. https://doi.org/10.3390/w11030550

Bui, V. H., Bui, M. D., & Rutschmann, P. (2019b). Combination of discrete element method and artificial neural network for predicting porosity of gravel-bed river. *Water*, *11*(7), 1461. https://doi.org/10.3390/w11071461

Carling, P. A. (1984). Deposition of fine and coarse sand in an open-work gravel bed. *Canadian Journal of Fisheries and Aquatic Sciences*, *41*(2), 263–270. https://doi.org/10.1139/f84-030

Cui, Y., Parker, G., Braudrick, C., Dietrich, W. E., & Cluer, B. (2006). Dam removal express assessment models (DREAM). *Journal of Hydraulic Research*, *44*(3), 291–307. https://doi.org/10.1080/00221686.2006.9521683

Cui, Y., & Wilcox, A. C. (2005). Numerical modeling of sediment transport upon dam removal: Application to Marmot Dam in Sandy River, Oregon. In: Sedimentation engineering, ASCE Manual 54, No. Vol. 2.

Cui, Y., Wooster, J. K., Baker, P. F., Dusterhoff, S. R., Sklar, L. S., & Dietrich, W. E. (2008). Theory of fine sediment infiltration into immobile gravel bed. *Journal of Hydraulic Engineering*, *134*(10), 1421–1429. https://doi.org/10.1061/(ASCE)0733-9429(2008)134:10(1421)

Cundall, P. A., & Strack, O. D. L. (1979). A discrete numerical model for granular assemblies. *Géotechnique*, *29*(1), 47–65. https://doi.org/10.1680/geot.1979.29.1.47

Diplas, P., & Parker, G. (1992). Deposition and removal of fines in gravel-bed streams. In: P. Billi, R. D. Hey, C. R. Thorne, & P. Tacconi (Eds.), *Dynamics of Gravel-Bed Rivers* (pp. 313–329). John Wiley.

Doyle, M. W., Stanley, E. H., & Harbor, J. M. (2003). Channel adjustments following two dam removals in Wisconsin. *Water Resources Research*, *39*(1), 1011–1025. https://doi.org/10.1029/2002WR001714

Einstein, H. A. (1968). Deposition of suspended particles in a gravel bed. *Journal of the Hydraulics Division*, *94*(5), 1197–1206. https://doi.org/10.1061/JYCEAJ.0001868

Evans, E., & Wilcox, A. C. (2014). Fine sediment infiltration dynamics in a gravel-bed River following a sediment pulse. *River Research and Applications*, *30*(3), 372–384. https://doi.org/10.1002/rra.2647

Frostick, L. E., Lucas, P. M., & Reid, I. (1984). The infiltration of fine matrices into coarse-grained alluvial sediments and its implications for stratigraphical interpretation. *Journal of the Geological Society*, *141*(6), 955–965. https://doi.org/10.1144/gsjgs.141.6.0955

Gibson, S., Abraham, D., Heath, R., & Schoellhamer, D. (2009). Vertical gradational variability of fines deposited in a gravel framework. *Sedimentology*, *56*(3), 661–676. https://doi.org/10.1111/j.1365-3091.2008.00991.x

Gimenez, J. M., Idelsohn, S. R., Oñate, E., & Löhner, R. (2021). A multiscale approach for the numerical simulation of turbulent flows with droplets. *Archives of Computational Methods in Engineering: State of the Art Reviews*, *28*(6), 4185–4204. https://doi.org/10.1007/s11831-021-09614-6

Harikrishnan, S., & Mahapatra, P. S. (2021). Effect of liquid–air interface on particle cloud dynamics in viscous liquids. *Physics of Fluids*, *33*(6), 63306. https://doi.org/10.1063/5.0048895

Herrero, A., & Berni, C. (2016). Sand infiltration into a gravel bed: A mathematical model. *Water Resources Research*, *52*(11), 8956–8969. https://doi.org/10.1002/2016WR019394

Herrero, A., Berni, C., Camenen, B., & Thollet, F. (2015). Laboratory analysis on silt infiltration into a gravel bed: Modélisation physique de l'infiltration dans un lit de graviers. https://hal.science/hal-01362697

Honjo, Y., & Veneziano, D. (1989). Improved filter criterion for cohesionless soils. *Journal of Geotechnical Engineering*, *115*, 75–94.

Huston, D. (2014). Clogging of fine sediment within gravel substrates: Macro-analysis and momentum-impulse model (These and Dissertation-Civil Engineering), Lexington, Kentucky. https://uknowledge.uky.edu/ce_etds/24

Indraratna, B., & Locke, M. R. (1999). Design methods for granular filters—Critical review. *Proceedings of the Institution of Civil Engineers—Geotechnical Engineering*, *137*(3), 137–147. https://doi.org/10.1680/gt.1999.370303

Indraratna, B., & Vafai, F. (1997). Analytical model for particle migration within base soil-filter system. *Journal of Geotechnical and Geoenvironmental Engineering*, *123*(2), 100–109. https://doi.org/10.1061/(ASCE)1090-0241(1997)123:2(100)

Iseya, F., & Ikeda, H. (1987). Pulsations in bedload transport rates induced by a longitudinal sediment sorting: A flume study using sand and gravel mixtures. *Geografiska Annaler Series A-Physical Geography*, *69*, 15–27.

Jaiswal, A., Bui, M. D., & Rutschmann, P. (2022). Evaluation of RANS-DEM and LES-DEM methods in OpenFOAM for simulation of particle-laden turbulent flows. *Fluids*, *7*(10), 337. https://doi.org/10.3390/fluids7100337

Johnson, K. L. (1987). Contact mechanics (1st pbk. ed. (with corrections)). Cambridge University Press. https://doi.org/10.1017/CBO9781139171731

Kenney, T. C., Chahal, R., Chiu, E., Ofoegbu, G. I., Omange, G. N., & Ume, C. A. (1985). Controlling constriction sizes of granular filters. *Canadian Geotechnical Journal*, *22*(1), 32–43. https://doi.org/10.1139/t85-005

Kloss, C., Goniva, C., Hager, A., Amberger, S., & Pirker, S. (2012). Models, algorithms and validation for opensource DEM and CFD-DEM. *Progress in Computational Fluid Dynamics, An International Journal*, *12*(2/3), 140. https://doi.org/10.1504/PCFD.2012.047457

Koch, D. L., & Hill, R. J. (2001). Inertial effects in suspension and porous-media flows. *Annual Review of Fluid Mechanics*, *33*(1), 619–647. https://doi.org/10.1146/annurev.fluid.33.1.619

Kuerten, J. G. M. (2016). Point-particle DNS and LES of particle-laden turbulent flow—a state-of-the-art review. *Flow, Turbulence and Combustion*, *97*(3), 689–713. https://doi.org/10.1007/s10494-016-9765-y

Latham, J. P., Munjiza, A., & Lu, Y. (2002). On the prediction of void porosity and packing of rock particulates. *Powder Technology*, *125*(1), 10–27. https://doi.org/10.1016/S0032-5910(01)00493-4

Lauck, T. (1991). A simulation model for the infiltration of sediment into spawning gravel (Master's thesis). Humboldt State University.

Lisle, T. E. (1989). Sediment transport and resulting deposition in spawning gravels, north coastal California. *Water Resources Research*, *25*(6), 1303–1319. https://doi.org/10.1029/WR025i006p01303

Lone, M. A., Hussain, B., & Asawa, G. L. (2005). Filter design criteria for graded cohesionless bases. *Journal of Geotechnical and Geoenvironmental Engineering*, *131*(2), 251–259. https://doi.org/10.1061/(ASCE)1090-0241(2005)131:2(251)

Loth, E. (2000). Numerical approaches for motion of dispersed particles, droplets and bubbles. *Progress in Energy and Combustion Science*, *26*(3), 161–223. https://doi.org/10.1016/S0360-1285(99)00013-1

Lunt, I. A., & Bridge, J. S. (2007). Formation and preservation of open-framework gravel strata in unidirectional flows. *Sedimentology*, *54*(1), 71–87. https://doi.org/10.1111/j.1365-3091.2006.00829.x

Minier, J. P., Chibbaro, S., & Pope, S. B. (2014). Guidelines for the formulation of Lagrangian stochastic models for particle simulations of single-phase and dispersed two-phase turbulent flows. *Physics of Fluids*, *26*(11), 113303. https://doi.org/10.1063/1.4901315

Minshall, G. W., Royer, T. V., & Robinson, C. T. (2001). Response of the Cache Creek macroinvertebrates during the first 10 years following disturbance by the 1988 Yellowstone wildfires. *Canadian Journal of Fisheries and Aquatic Sciences*, *58*(6), 1077–1088. https://doi.org/10.1139/f01-056

Nan, X., Shen, Z., Hou, J., & Li, G. (2023). High-resolution model of complexly shaped bodies motion using an IBM-VOF-DEM coupling method. *Powder Technology*, *413*, 118005. https://doi.org/10.1016/j.powtec.2022.118005

NCASI. (1981). *Factors affecting changes in the percent of fine sediment in gravel bedded channels* (No. Technical Bulletin No. 0354). NCASI.

Parker, G., Cui, Y., Imran, J., & Dietrich, W. E. (1996). Flooding in the lower Ok Tedi, Papua New Guinea due to the disposal of mine tailings and its amelioration. In: International Seminar on Recent Trends of Floods and Their Preventative Measures, Hokkaido Disaster Prevention Research Center.

Pollard, A. I., & Reed, T. (2004). Benthic invertebrate assemblage change following dam removal in a Wisconsin stream. *Hydrobiologia*, *513*(1), 51–58. https://doi.org/10.1023/B:hydr.0000018164.17234.4f

Sakthivadivel, R., & Einstein, H. A. (1970). Clogging of porous column of spheres by sediment. *Journal of the Hydraulics Division*, *96*(2), 461–472. https://doi.org/10.1061/JYCEAJ.0002332

Schälchli, U. (1992). The clogging of coarse gravel river beds by fine sediment. *Hydrobiologia*, *235–236*(1), 189–197. https://doi.org/10.1007/BF00026211

Schuler, U., & Brauns, J. (1993). Behaviour of coarse and well-graded filters. In: J. Brauns, M. Heibaum, & U. Schuler (Eds.), *Filters in Geotechnical and Hydraulic Engineering* (pp. 3–18). Balkema.

Sherard, J. L., & Dunnigan, L. P. (1986). Filters and leakage control in embankment dams. *International Journal of Rock Mechanics and Mining Sciences & Geomechanics Abstracts*, *23*(5), 202. https://doi.org/10.1016/0148-9062(86)90266-4

Sherard, J. L., & Dunnigan, L. P. (1989). Critical filters for impervious soils. *Journal of Geotechnical Engineering*, *115*, 927–947.

Stanley, E. H., Luebke, M. A., Doyle, M. W., & Marshall, D. W. I. (2002). Short-term changes in channel form and macroinvertebrate communities following low-head dam removal. *Journal of the North American Benthological Society*, 21, 172–187.

Sundar, V., & Sannasiraj, S. A. (Eds.). (2019). *Advanced series on ocean engineering: Volume 47. Coastal engineering: Theory and practice*. World Scientific Publishing Co. Pte. Ltd. https://doi.org/10.1142/ASOE

Swanson, F. J., & Dyrness, C. T. (1975). Impact of clear-cutting and road construction on soil erosion by landslides in the western Cascade Range, Oregon. *Geology*, 3(7), 393. https://doi.org/10.1130/0091-7613(1975)3<393:IOCARC>2.0.CO;2

Vieira, N. K. M., Clements, W. H., Guevara, L. S., & Jacobs, B. F. (2004). Resistance and resilience of stream insect communities to repeated hydrologic disturbances after a wildfire. *Freshwater Biology*, 49(10), 1243–1259. https://doi.org/10.1111/j.1365-2427.2004.01261.x

Washino, K., Chan, E. L., Tsujimoto, T., Tsuji, T., & Tanaka, T. (2023). Development of resolved CFD–DEM coupling model for three-phase flows with non-spherical particles. *Chemical Engineering Science*, 267, 118335. https://doi.org/10.1016/j.ces.2022.118335

Wooster, J. K., Dusterhoff, S. R., Cui, Y., Sklar, L. S., Dietrich, W. E., & Malko, M. (2008). Sediment supply and relative size distribution effects on fine sediment infiltration into immobile gravels. *Water Resources Research*, 44(3), W03424. https://doi.org/10.1029/2006WR005815

Yu, A. B., & Standish, N. (1991). Estimation of the porosity of particle mixtures by a linear-mixture packing model. *Industrial & Engineering Chemistry Research*, 30(6), 1372–1385. https://doi.org/10.1021/ie00054a045

Yu, A. B., & Standish, N. (1993). Limitation of proposed mathematical models for the porosity estimation of nonspherical particle mixtures. *Industrial & Engineering Chemistry Research*, 32(9), 2179–2182. https://doi.org/10.1021/ie00021a043

Yu, A. B., Zou, R. P., & Standish, N. (1996). Modifying the linear packing model for predicting the porosity of nonspherical particle mixtures. *Industrial & Engineering Chemistry Research*, 35(10), 3730–3741. https://doi.org/10.1021/ie950616a

Zhou, Z. Y., Kuang, S. B., Chu, K. W., & Yu, A. B. (2010). Discrete particle simulation of particle–fluid flow: Model formulations and their applicability. *Journal of Fluid Mechanics*, 661, 482–510. https://doi.org/10.1017/S002211201000306X